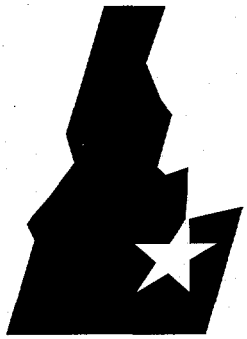

Idaho
National
Engineering
Laboratory

INEL/EXT-97-00319
April 1997

# INEEL BNCT Research Program Annual Report 1996



*Edited by*
*J. R. Venhuizen*



LOCKHEED MARTIN

INEL/EXT-97-00319

# INEEL BNCT Research Program
# Annual Report
# 1996

**Edited by**
**J. R. Venhuizen**

**Published April 1997**

**Idaho National Engineering and Environmental Laboratory**
**Lockheed Martin Idaho Technologies Company**
**Idaho Falls, Idaho 83415**



**Prepared for the**
**U.S. Department of Energy**
**Office of Energy Research**
**Under DOE Idaho Operations Office**
**Contract DE-AC07-94ID13223**

# ABSTRACT

This report is a summary of the progress and research produced for the Idaho National Engineering and Environmental Laboratory (INEEL) Boron Neutron Capture Therapy (BNCT) Research Program for calendar year 1996. Contributions from the individual investigators about their projects are included, specifically, physics: treatment planning software, real-time neutron beam measurement dosimetry, measurement of the Finnish research reactor epithermal neutron spectrum, BNCT accelerator technology; and chemistry: analysis of biological samples and preparation of $^{10}B$ enriched decaborane.

## DISCLAIMER

# CONTENTS

# FIGURES



# TABLES

# ACRONYMS AND ABBREVIATIONS

| | |
|---|---|
| ADC | analog-digital-converter |
| BNCT | Boron Neutron Capture Therapy |
| BNL | Brookhaven National Laboratory |
| BSH | borocaptate sodium |
| CHNS | carbon hydrogen nitrogen sulfur |
| CRADA | Cooperative Research and Development Agreement |
| DICOM3 | magnetic tape format |
| DOE | Department of Energy |
| DORT | Discrete Ordinate Radiation Transport |
| eV | electron volt |
| FTIRS | Fourier transform infrared spectroscopy |
| GC | gas chromatography |
| GC-AED | gas chromatography w/atomic emission detection |
| GC-TCD | gas chromatography w/thermal conduction detection |
| Gy | gray-unit of radiation exposure |
| HPLC | high-pressure liquid chromatography |
| HQ-ER | Head Quarters-Energy Research |
| HTML | hyper-text markup language |
| HVPS | high voltage power supply |
| ICP-AES | inductively coupled plasma-atomic emission spectrometry |
| INEEL | Idaho National Engineering and Environmental Laboratory |
| IR | infrared spectroscopy |
| IST | International Sensor Technology |
| ISU | Idaho State University |
| keV | kilo-electron volt |
| kW | kilo-watt |
| LBNL | Lawrence Berkeley National Laboratory |
| LMITCO | Lockheed Martin Idaho Technologies Company |
| MC | Monte Carlo |
| MCNP | Monte Carlo N-particle |
| MeV | million electron volt |
| MIT | Massachusetts Institute of Technology |
| MSU | Montana State University |
| NCAR | National Center for Atmospheric Research |
| MW | megawatt |
| NMR | nuclear magnetic resonance |
| NURBS | Non-uniform Rational B-spline |
| OSU | Ohio State University |

| | |
|---|---|
| PC | personal computer |
| PI | Principal Investigator |
| PMT | photo-multiplier tube |
| PNNL | Pacific Northwest National Laboratory |
| QA/QC | quality assurance/control |
| QSH | magnetic tape format |
| Rpte | Radiation treatment planning environment |
| rtt | radiation transport in tissue |
| TIDBIT | The INEEL Database of BNCT Information and Treatment |
| TLD | thermolouminescent dosimeter |
| TRIGA | Transient Reactor Irradiator-General Atomics |
| UCD | University of California, Davis |
| UCLA | University of California, Los Angeles |
| UCSF | University of California, San Francisco |
| UofI | University of Iowa |
| UofU | University of Utah |
| UofW | University of Washington |
| URL | universal resource locator |
| VTT | Valtion Teknillinen Tutkimuskeskus |
| WSU | Washington State University |

# INEEL BNCT RESEARCH PROGRAM ANNUAL REPORT 1996

## INTRODUCTION

The Idaho National Engineering and Environmental Laboratory (INEEL) Boron Neutron Capture Therapy (BNCT) Research Program completed its 10th year as a Department of Energy (DOE) funded program with a continuing increase in interest from the medical community. This interest, in the form of a Cooperative Research and Development Agreement (CRADA), represents a move of the INEEL research from the national laboratory setting into the private sector. Interest from the international community in the INEEL treatment planning software has prompted the Program Office to offer several forms of license agreements: Class D for DOE Laboratories, unrestricted research use; Class B, Beta test sites, most likely universities, no human use allowed; Class R, research use, possibly for humans, compensation from the facility required to cover INEEL costs of providing the software and personnel support; Class C, commercial use for profit, currently specific rights assigned by license agreements to the CRADA partner. The Program goals remain: to move BNCT into a clinically useful therapy through applications of supportive research, and support the DOE national program via assistance with DOE grantees and the Brookhaven National Laboratory (BNL) clinical trials.

In the course of the year, assistance to other national laboratories was provided via program reviews and transmittal of the treatment planning software for non-human use. Dr. David Nigg, as requested by DOE-HQ-ER, participated in the Lawrence Berkeley National Laboratory (LBNL) BNCT Site Visit Program review. Both BNL and LBNL physicists have been trained in the use of the INEEL treatment planning software, which has been installed at both sites.

The Program has invested in research to synthesize $^{10}B$ enriched decaborane, a precursor for several advanced boron agents currently of interest. There is no known current manufacturing capability in the U.S. for this important product, and the synthesis route is sufficiently difficult to warrant a national laboratory to investigate and develop a new method. A total of 300 grams was produced and delivered to an offsite laboratory for processing into a final form advanced experimental boron agent. The synthesis process developed is sufficiently different from that reported in the literature to warrant new patent applications for the synthesis. Analytical chemistry support was also provided to the other DOE grantees as well as INEEL activities. An excess of 4,100 biological samples from all participants were analyzed for boron content.

During 1996, development and refinement of the BNCT radiation treatment planning environment (BNCT_Rtpe) software continued under the version 2.2 preliminary release. In addition, development continued on several existing and new fronts, including the BNCT dose display tool, a new user interface, expanded image format and display handling utilities, and a Java-based demonstration/tutorial of BNCT_Rtpe. Versions of BNCT_Rtpe and the dose display tool are now available for Intel processors under the Linux 2.0 and Solaris X86 operating systems. Work has continued for the particle transport code used in the treatment planning system to include neutron energies up to 100 MeV, required to support accelerator generated neutron beams for fast-neutron therapy with BNCT augmentation. Also, the patient-beam optimization problem- how to orient the patient with respect to the neuron beam- has been investigated, and a possible computational model developed. Reports on all these refinements are included in this report.

During the year, three INEEL scientists visited the Finnish research reactor FiR1 as part of a long-standing collaboration between INEEL and

the Finnish BNCT Program to measure the epithermal-neutron spectra for that reactor. A complete report of this activity is included. The radiation measurement capability of the INEEL was further enhanced by procurement of a new thermoluminescent dosimeter (TLD) reader. A short report of this capability is included this report. Additional measurements of the fiber optic neutron detector were taken at the Washington State University (WSU) research reactor to support the real-time neutron measuring project. A joint experiment with Pacific Northwest National Laboratories (PNNL) scientists was conducted with the assistance of a visiting scientist from Thailand. A short report of these experiments is included.

The database program, reported on in some detail in the Program's 1994 Annual Report, has been in beta testing with both animal and human data entered in separate files. An update on this program is included in this report. The program, TIDBIT (The INEEL Database of BNCT Information and Treatment), is also available to other DOE Laboratories and grantees for unrestricted research use. Access to the program is via the Internet.

INEEL BNCT Program participants presented three papers at the Seventh International Symposium on Neutron Capture Therapy for Cancer in September 1996 in Zurich, and were co-authors on 9 other papers.

This publication summarizes the research accomplished during calendar year 1996. References are included at the end of each section for that particular section.

# LABORATORY SYNTHESIS OF $^{10}B$ ENRICHED DECABORANE

**R. L. Cowan (INEEL)**

Decaborane ($B_{10}H_{14}$) is arguably the most useful synthetically derived boron hydride cage compound. It is air-stable yet remains reactive toward chemical substitution and derivatization. In these respects, it is an ideal precursor for many potential BNCT boron agents. There is, however, no longer a domestic supplier of this valuable resource. Because of the inability to purchase this material, INEEL scientists have undertaken the task of developing a synthetic strategy beginning with boric acid which can yield decaborane with at least 90 to 95% isotopic purity.

The method chosen to investigate the synthesis of decaborane was solution-based and did not require pressurized reaction vessels, thus rendering it as a relatively safe route for laboratory use. In order for decaborane to be useful for BNCT boron agents, it must be enriched in the $^{10}B$ isotope. The starting material, $^{10}B$-enriched boric acid, is available commercially and is fairly inexpensive. (The boric acid is obtained as a by-product from defense-related semiconductor industry, which prefers to have the $^{11}B$-isotope due to its radiation stability. The $^{10}B$-isotope, because of its ability to capture thermal neutrons, is the preferred isotope for BNCT therapy.) The $^{10}B$-enriched boric acid is transformed, through a series of 4 synthetic steps, into the desired decaborane product. The synthetic procedure utilizes modified literature[1-6] methods, which provide for complete retention of the $^{10}B$ label in the final product. The synthesis uses standard laboratory glassware and can be performed in any normal synthetic laboratory. The product is obtained as a solution which analyzes about 93-95% pure.

**REFERENCES:**


1. H.I. Schlesinger, H. C. Brown, D.L. Mayfield and J.R. Gilbreath, "Procedures for the Preparation of Methyl Borate", *J. Amer. Chem. Soc., 75*, 213 (1953).

2. H.I. Schlesinger, H.C. Brown and A.E. Finholt, "The Preparation of Sodium Borohydride by the High Temperature Reaction of Sodium Hydride with Borate Esters", *J. Amer. Chem. Soc., 75*, 205 (1953).

3. W.S. Fedor, M.D. Banus and D.P. Ingalls, "Potassium Borohydride Manufacture", *Ind. Eng. Chem., 49*, 1664 (1957).

4. B.D. James and M.G.H. Wallbridge, "Metal Tetrahydrobrates", *Prog. Inorg. Chem., 11*, 99 (1970).

5. G.B. Dunks, K. Barker, E. Hedaya, C. Hefner, K. Palmer-Ordoñez and P. Remec, "Simplified Synthesis of $B_{10}H_{14}$ from $NaBH_4$ via $B_{11}H_{14}^-$ Ion", *Inorg Chem., 20*, 1692 (1981).

6. G.B. Dunks, K. Palmer-Ordoñez and E. Hedaya, "Decaborane(14)", *Inorg. Synthesis, 22*, 202 (1983).

# ANALYTICAL CHEMISTRY SUPPORT

W. L. Bauer (INEEL)

During 1996, there were basically three analytical chemistry related functions. The first of these functions was simply the determination of boron in a variety of biologically related samples using inductively coupled plasma atomic emission spectroscopy (ICP-AES). The second two analysis functions were related to quality assurance/control (QA/QC) of sodium borocaptate (BSH) for use in clinical trials, and for the synthesis of $^{10}B$ enriched decaborane.

## DETERMINATION OF BORON IN BIOLOGICAL SAMPLES

During 1996, 4,154 biological samples were received and assayed for boron content. Of these, 2,813 were from dogs and/or rodents from the BNCT related programs at WSU (Dr. P. Gavin, Principal Investigator (P.I.)); 91 were of stock solutions to be sent to WSU and assorted other preparations from the program at University of California, Los Angeles (UCLA) (Dr. M. F. Hawthorne, P.I.); 157 were from close-out activities at Idaho State University (ISU) (Dr. T. LaHann, P.I.); 132 were from close-out activities at University of Utah (UofU) (Dr. M. Schweizer, P.I.); 312 were from the BNCT research group at University of California, San Francisco (UCSF) (Dr. S. Kahl, P.I.); and 649 were from the program at LBNL (Dr. D. Dean, P.I.). During FY-97, additional samples are expected from UCLA, WSU, UCSF and LBNL. Samples are also expected from BNCT related activities at Massachusetts Institute of Technology (MIT) (Dr. J. Yanch, P.I., Synovectomy program), University of Washington (UofW) (Dr. G. Laramore, P.I., BNCT boost to fast neutron therapy), and the University of California, Davis (UCD) (Dr. J. Boggan, P.I.).

## QA/QC ANALYSES OF BSH

The QA/QC analyses of BSH during 1996 were primarily related to the effort at Ohio State University (OSU) to get Phase I clinical trials initiated using BSH. The BSH was natural abundance boron and originally purchased by OSU from Centronics, Ltd. (England). The analyses work consisted of initial characterization using high pressure liquid chromatography (HPLC) as the primary analysis tool. The initial characterization also included $^{10}B/^{11}B$ nuclear magnetic resonance (NMR) spectroscopy, Fourier transform infrared spectroscopy (FTIRS), ICP-AES, and carbon, hydrogen, nitrogen and sulfur analysis with a CHNS analyzer. After the initial characterization, the BSH was sent to Dr. R. Poust at the University of Iowa (UofI) for "final form" packaging. INEEL support continued by using HPLC to verify that the "packaging process" did not cause significant oxidation of the BSH. ICP-AES analysis for boron on some swabs was also performed to verify that the equipment was clean at the UofI.

Once the BSH product had been "final form" packaged, a shelf-life study was initiated. In this study, two "final form" packaged BSH vials were analyzed each month to verify that there was no significant degradation/oxidation products. Once initiated, some minor oxidation was noted, and it was discovered that there was significant oxygen (air) in the headspace of the final form vials. This initiated a series of samples for oxygen analysis by gas chromatography (GC) of vial headspace as UofI researchers tried to alleviate this situation. All of the remaining vials were ultimately reprocessed by the UofI and the shelf-life studies reinitiated. Determination of the oxidation product level in the BSH solid and GC analysis of the vial headspace for oxygen content are now standard practices during these most recent, and still on-going, shelf-life studies.

## QA/QC ANALYSES FOR DECABORANE SYNTHESIS

Analytical method development and documentation to support the decaborane synthesis project was also performed in 1996, and will be continued into 1997. Methods of analysis for all of the major process steps and intermediate product are being developed, performed and documented. Methods will include analysis of methoxyborate, isolated and in the azeotropic mixture, with GC and possibly by infrared spectroscopy (IR). Analysis of the sodium borohydride product is performed by a standard redox titration method and ICP-AES is used to correlate the boron content to verify that it is borohydride. The decaborane reaction sequence is monitored with $^{10}B$ NMR, and the final product quantitated with GC with thermal conductivity detection (GC-TCD). The GC-TCD analysis of decaborane was verified by comparison to results generated using GC with atomic emission detection (GC-AED). Refinements to these methods and further method development are being continued into 1997.

# BNCT-Rtpe: BNCT RADIATION TREATMENT PLANNING ENVIRONMENT

**D. E. Wessol[1], R. S. Babcock[2], N. Esty[2], M. Frandsen[2], G. Harkin[2], D. Starkey[2], L. Voss[2], and F. J. Wheeler[1] [1- INEEL, 2- Montana State University (MSU)]**

During 1996, development and refinement of BNCT_Rtpe continued under the version 2.2 preliminary release. Additionally development continued on several existing and new fronts including 'xcontours'- the BNCT dose display tool; a new user interface to rtt_MC (MC-Monte Carlo); expanded image format and display handling utilities; and a Java-based demonstration/tutorial of BNCT_Rtpe. Versions of BNCT_Rtpe and 'xcontours' are now available for Intel processors under the Linux 2.0 and Solaris X86 operating systems (UNIX-like operating systems for the Intel processor).

## ITEMIZED REFINEMENT OF BNCT_RTPE VERSION 2.2

Many modifications and new features were added to BNCT_Rtpe during 1996. Some of these features are delineated below:

- Developed scrollable image container widget for BNCT_Rtpe. All the images used in a treatment plan are now contained in a single widget, and the images can be scrolled either horizontally or vertically. In addition to the scroll bars, a list of axial locations can be used to navigate about the image array.
- Moved context sensitive help files into a subdirectory named 'helpdir' in the BNCT resources directory.
- Changed 'histo' to ignore the first two columns found in the rtt_MC output so that the dose volume histograms are referenced to the total dose.
- Several modifications were made to the rtt_MC (radiation transport in tissue-Monte Carlo) post processor, 'rttPP', including a button and popup to force user to enter the date in the correct format.
- Changed the edit body selection of BNCT_Rtpe so that curves are continuously updated as the points are moved. This provides the user a better sense of how the control point location affects the curve fit and shape.
- Modified the 2X image magnification option so that it can not be called in the middle of an operation, such as the 'New Body' operation. Also, new body names are forced to be unique when they are entered.
- Fixed loading in QSH (magnetic tape image format) files so that the minimum and maximum axial (Z) values are set according to the data in the QSH header file if this key is present.
- Cleaned out redundant codes and objects from the BNCT_Rtpe directory tree which remained after the replacement of the Non-uniform Rational B-Spline (NURBS) coding.
- Forced control points to be entered in a clockwise fashion.
- Changed border around images so that Z values are now enclosed inside the border to avoid confusion.
- Improved the edge detection paradigm that allows edge detection for one body on multiple slices consecutively.

## DOSE CONTOURING

The BNCT dose contouring tool, which displays the rtt_MC dose data, has been improved to the to take advantage of the multiple image widget. Rather than viewing just one slice and an associated dose component, multiple slices can be viewed in a variety of ways: The same dose component can be viewed on multiple slices, multiple copies of one slice can be viewed with each showing a different component, or other variations are possible. When a dose component is selected, or any other operation that affects the displayed contours is selected, it can either be applied to the active image or to the entire set of images. Masking operations can be performed as before by applying the mask to an individual slice, or the user can now apply the mask to the corresponding region in all image slices. An option has been added which allows the display of either the mask or the standard medical grayscale image in the image widget. A time saving feature, called the 'Smart Loader', has been added, which greatly automates the task of loading an image set. Finally the maximum, increment, and number of contours levels are printed below the magnified image, and an annotated text area is provided below the multiple image widget. By default the text area must be shown by pulling up on the sash button located near the bottom right hand corner of the multiple image widget.

## IMAGE HANDLING

Improvements and refinements were made to the QSH conversion utility 'toQsh'. The graphical user interface has been altered and now has the same style menus, look, and feel as found in BNCT_Rtpe and 'xcontours'. Minor changes reflect the standardization of some keys and the agreed upon minimum set of necessary keys. The QSH utility has been expanded to allow the image set to be re-sized and/or rotated. Additionally, the user is presented with lists of both the recognized key/value combinations and those that are either unnecessary or not recognized; these lists can be used to quickly verify integrity of an alias operation, identify new aliases, and to help fill in any necessary header information that is missing. The required set of keys is as follows:

Required Global Keys

| | |
|---|---|
| Bytes per pixel | integer |
| Byte order | "little endian" \| "big endian" (if bpp!=1) |
| Pixel format | integer |
| Dimensionally | "mm" \| "cm" \| "in" |
| Number of dimensions | integer |
| Size of dimension[0\|1\|2] | integer |
| X Pixel Size | float |
| Y Pixel Size | float |
| Uniform Thickness | float |
| Reference Location | float |
| Minimum Pixel Value | integer |
| Maximum Pixel Value | integer |
| Modality | "CT" \| "MRI" \| "NMR" |

Required Local Keys

| | |
|---|---|
| Minimum Pixel Value | integer |
| Maximum Pixel Value | integer |
| Image Location | float |

If all standards are followed, include: Version: = 2

When these keys are not present in the header file, 'toQsh' will prompt the user to enter values for these keys. DICOM3 (magnetic tape image) format conversion functions were written for 'toQsh' but have not been incorporated at this time.

## rtt_MC INTERFACE DEVELOPMENT

The original version of the rtt_MC popup design was completed and implemented as is shown in Figure 1.

The Edit Directives section has provided an easy to use and efficient method to interactively insert these items into an rtt input data file. The option to run the rtt_MC program from this popup was implemented. Many ideas for data entry were evaluated and rejected before settling on the current design. Extensive use of the standard text editing techniques provided by X11/Motif allowed a similar look and feel for the rtt popup as in other parts of the BNCT_Rtpe software. Future activity will continue to refine and develop this interface as it is tried and tested by BNCT_Rtpe users. Monitoring the running of the rtt program with this popup will be implemented and tested.

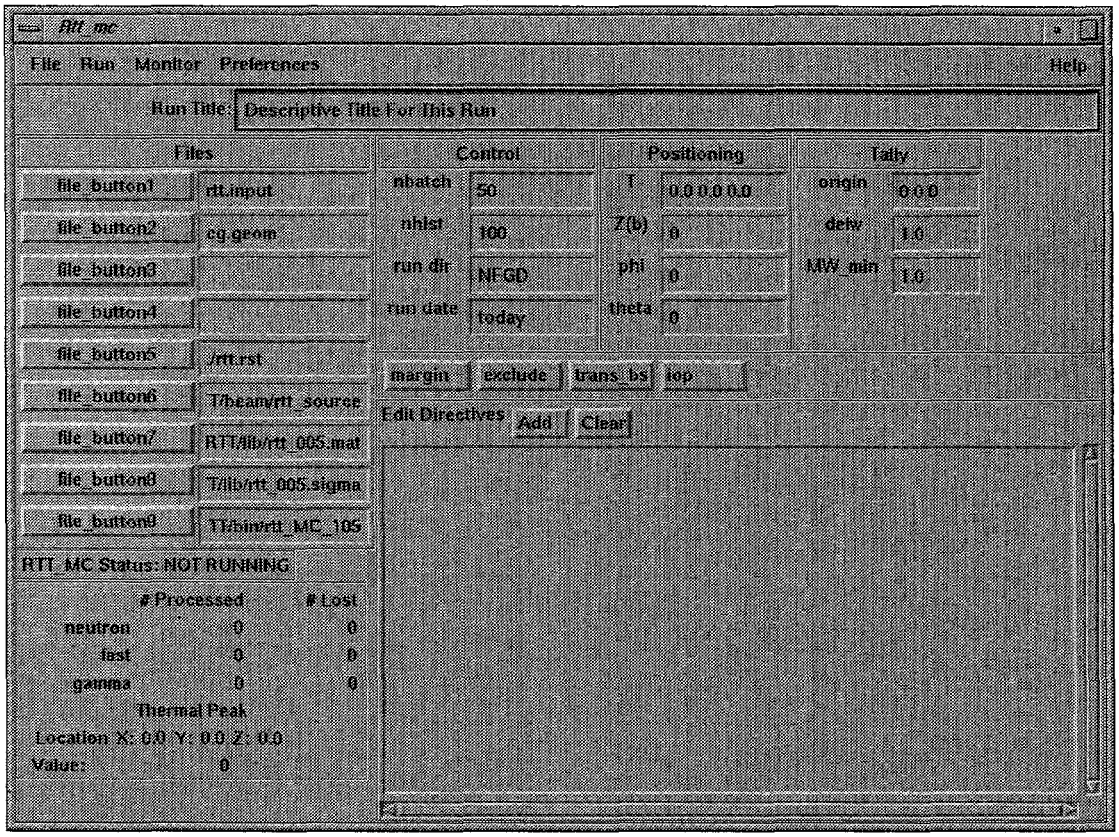


**Figure 1.** Menu popup for rtt_MC.

## JAVA-BASED DEVELOPMENT

Efforts are underway to explore the viability of creating a Java-based version of BNCT_Rtpe. Towards that end a demonstration version of BNCT_Rtpe has been written and can be accessed using a Java compatible web browser and the universal resource locator (URL) http://www.cs.montana.edu:80/people/bnct. The demonstration uses the same basic layout as the main BNCT_Rtpe program and contains an extensive help system so that this demonstration can be used instructively. The advantages of Java are considerable, including machine transparency, maintaining only a single version of the software, and easy distribution. All the user would need is a Java-compatible web browser to run BNCT_Rtpe. In the near term it is unlikely that rtt_MC will prove to be viable under a Java-based system.

## WORK IN PROGRESS

Mike Frandsen (Doctoral student at MSU) has commenced work on his thesis research that centers on the development of methods to automatically label and segment the medical images into the various volume components, and the development of highly efficient algorithms for computing ray intersections with the resultant bodies. The automatic segmentation algorithms will attempt to find regions of interest with minimum user intervention; the user will, of course, be given the option of approving or refining the resultant segmentation. This should prove to be time-saving and improve the consistency (and reproducibility) of resultant plans. Improved computation of intersections of a ray with various bodies will speed the Monte Carlo transport simulations that track the neutron beam.

Continuous refinement and feature development are being implemented in BNCT_Rtpe including the rtt_MC interface. Plans are to have the BNCT_Rtpe development under a commercial software configuration and management package in 1997. Requests for a 64 bit version of BNCT_Rtpe have been made and resources are being allocated for this effort. A version 2.3 release is scheduled for late summer 1997.

One of the big pushes for 1997 will be development of a non-proprietary set of contouring utilities to replace the National Center for Atmospheric Research (NCAR) libraries. Both two and three dimensional dose contours and displays will be addressed, and it is hoped to have the two dimensional contours completed by the end of 1997. The new contour functions will be syntactically similar to the NCAR functions to minimize their incorporation into 'xcontours'. Contouring software libraries written specifically for this problem will lead to more control over the contouring functions, which in turn will allow significant improvements in 'xcontours'.

Most of the BNCT_Rtpe manual has been converted to hyper-text markup language (HTML) and will be soon available on the World Wide Web, most likely in the same location as the Java demonstration.

# THE rtt_MC SOFTWARE MODULE FOR TREATMENT PLANNING

**F. J. Wheeler, D. E. Wessol, and C. E. Wemple (INEEL)**

The rtt_MC software module[1] represents an improvement in treatment planning software. This module simulates neutron and gamma transport in a geometry model based on BNCT_Rtpe image reconstruction or on analytical solid regions and presents flux and dose patterns in zero, one, two, or three dimensional forms. Early versions of this software are currently in use in the BNL BNCT clinical trials and will be used in the European BNCT clinical trials at the Petten facility in The Netherlands. This software has also been installed at several other research facilities for evaluation and use as a research tool.

This module is still under development and new versions are periodically released for use following extensive validation and verification testing. New features that have recently been implemented in version 106 include:

- options to exclude any region(s) of the model, allowing for more efficient transport calculations with less surface intersection error but still allowing edits for the excluded region(s).
- incorporation of experimental software which allows rapid computations of "two-field" dose patterns for use in developmental optimization methods.
- an option to create three-dimensional dose data files for use in 3D graphical display software programs such as the IBM "Data Explorer".
- the ability to generate contour data and region masks for a "beam plane" where a beam plane can be oblique to the image slices.
- allowance of a reference "tolerance" volume other than the default 1 $cm^3$ volume of an edit voxel which can be specified to be located only in a list of acceptance regions.
- more interaction with the BNCT_Rtpe reconstruction software module.
- an edit directive which makes it more automatic to generate multiple contour file sets with minimum input data.
- an edit directive which generates a dose/volume histogram with minimum input specification.

Details on each of these features follows:

**Exclude option for transport calculations**

Frequently, volumes are defined in the model which do not effect particle transport since they do not affect the composition spatial distribution. These regions might be a functional segment of the brain such as the optic chiasm or an edit region such as a target margin around a tumor. Since the region contains the identical composition as the surrounding structure, the neutron or gamma flux will not be affected by exclusion of the region. Of course, each added region requires more computation time and introduces more possibilities of surface overlap problems where pseudo particles may get "lost" during the radiation transport simulation.

The rtt_MC interface menu popup widget (shown on Figure 1 of this report) has a button labeled "exclude" near the center of the widget. When this button is pressed, a popup requests a list of region names. Names entered on that list are excluded from the geometry during setup and transport, and re-included during post-transport editing. Since the region edits are obtained during the transport simulations, the region edits will correspond to the geometry without these 'excluded' regions.

**Rapid computation for "two-field" dose patterns**

The rtt_MC module has a fast 'table lookup' mode as an experimental option. A rigorous Monte Carlo simulation may be run for any geometric model and a dose table file specified to be created by using the 'Bopt' edit directive. Subsequently, a run may be made in 'T' mode specifying that the dose tables generated in the Monte Carlo run be used as an estimate for dose for the 'T' run. The approximation is made that the dose is a Lagrangian fit to depth from outer surface and radius from the beam center line. For single-field cases it has also been possible to perform a simple grid-search optimization calculation to find the single field providing the best dose pattern in a target. Comparisons with follow-up Monte Carlo calculations have found this search option to be quite accurate for specifying beam orientation.

The optimization process for single field is not too difficult. A skilled planner can find the best beam orientation quite rapidly for the single field case based on an intuition-aided trial and error search. For more than one field, however, the trial and error approach becomes unwieldy and intuition does not generally guide one to the best beam orientations. Therefore, an edit directive 'beam_N' has been added, which allows one to specify a second field in addition to the primary field specified as usual in the rtt_MC run. This edit directive is valid only for 'T' mode and the total number of fields is presently limited to two, although it is possible to add more fields in the future if this proves useful. With this option, it is possible to rapidly approximate two-field cases and find the match which compromises between the target dose pattern and healthy tissue constraint. Computer time requirement is only about one minute per two-field calculation.

There is not an automated optimization built into rtt_MC for the two-field case, and a simple grid-search scheme is not very efficient for the two-field case. Under development are optimization methods based on more sophisticated techniques (e.g. gradient method) using external software. This development is being performed by Dr. Mark Landon (INEEL). Results of these developments will be published when available.

**Generation of data for three-dimensional displays**

It is possible to generate three-dimensional data displays with a three-dimensional visualizer such as the IBM Data Explorer package (DX). The DX3d edit directive causes the required three-dimensional data set to be written to a file. INEEL does not provide the three-dimensional viewer or the drivers at this time, but three-dimensional displays have been generated at BNL by Ballard Andrews using DX. For an example, see Figure 2.

**Beam-plane edit**

A request was received for generation of region-mask image and contour data corresponding to a plane determined by the beam center line. Up to this point it was easy to generate contours for slices parallel to the image slices used in the reconstructions and possible to generate contours perpendicular to those image planes, but not possible to generate data for oblique planes. With this option, oblique planes are generated with little difficulty in required input. Also desired were depth dose plot data at the edge of the beam. Both of these are implemented with the 'beamplt' edit directive, with an example being:

beamplt 40 40 1 24.0 6.0 oblique

This instruction will cause generation of a 40 by 40 array of contour data to be written to the file 'oblique,contour' and a region mask raster file generated as 'oblique,mask'. The field of view in this case would be 24.0, and the plane orientation is specified by the third integer. Also, a dose/depth plot would be generated at 6.0 cm on both sides of the beam line in the contour plane.

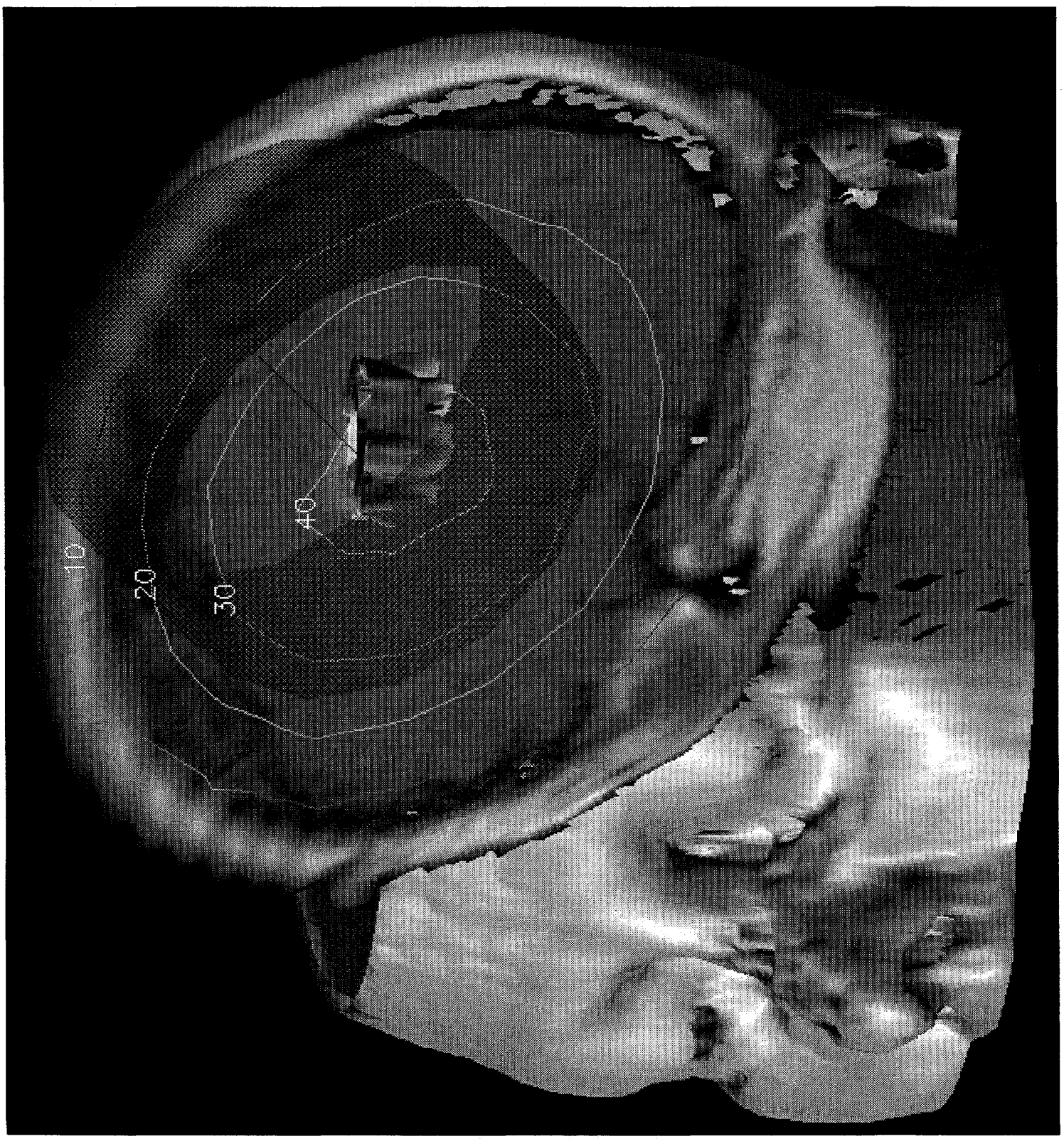


**Figure 2.** Example of a three dimensional display of image reconstruction and contour data. This figure courtesy of Ballard Andrews, BNL.

**Specification of reference tolerance volume**

The default reference volume is the volume of one edit voxel, 1.0 $cm^3$. It may be desirable to specify a large reference volume. For example, in conventional radiotherapy, the 90% isodose contour interval is sometimes used for the prescribed dose. Thus, there may be a substantial volume of healthy tissue which receives a dose greater than or equal to that at the 90% isodose level. With the new edit directives 'refvol' and 'ref_reg', it is possible to specify a large reference volume and to also specify that this volume resides within the region list specified by the 'ref_reg' edit directive.

**Interaction with BNCT_Rtpe**

As stated on pages 10 and 11, there are several tools in the BNCT_Rtpe module for interacting with rtt_MC. The primary output from BNCT_Rtpe, of course, are the geometry files with suffixes .rs and .rm. Now being implemented is the interface widget, shown in Figure 1, for preparing input to rtt_MC. The user may begin with the built in defaults or use an existing input file as a template for preparing input for a new run. All input is now prepared easily using buttons and pull down menus, and an edit window for the edit directives. After the input is prepared, the user can make a test run. This test run causes a setup and execution of a specified (small) number of particle histories. During the test run, the particle tracks are written to a file named 'rtt_tracks'. This file may be used to display the tracks in the BNCT_Rtpe reconstruction window where they are labeled depending on the particle type and energy. During a normal run, rtr_MC_106 writes two temporary files. The file 'rtt_mon' shows the current status and the number of histories tracked and 'lost'. The monitor on the interface widget reflects this information. The module also writes a file 'history' which shows the beam line and lost tracks. When there are geometry problems resulting in lost particles, it can be very useful to enter the 'history' file into the reconstruction window and display the lost tracks.

**Multiple contour data sets with the 'ottocon' edit directive**

The 'ottocon' edit directive was added to make it possible to generate a series of region-mask images and associated contour data sets. If following a certain convention for relating image space to model space, it is not required to specify a geometry transform. All that is required an appropriate '.rs' file is being used for the geometry specification and a line such as:

ottocon 40 40 target

This instruction will cause contours to be generated in a 40 by 40 array for every 'Z slice' intersecting the target as specified in the '.rs' geometry file.

**Dose/Volume histogram obtained with the 'DVbs' edit directive**

When using geometry specified with the '.rs' file from BNCT_Rtpe, it is now very easy to obtain a dose/volume for a region or set of regions. The appropriate boron concentrations, RBE factors, etc., are specified and the desired regions are listed to be included in the integration using the 'in_reg' edit directive. The dose/volume integration is then obtained with the line:

DVbs

No input data are required on the 'DVbs' line. The bounding box limiting the integration range is found using the control points and 'Z' values in the '.rs' file and the integration is performed.

## REFERENCES

1. F. J. Wheeler, Radiation Transport in Tissue by Monte Carlo, EGG-BNCT-11178, January, 1994.

# HIGH ENERGY MONTE CARLO TRANSPORT CALCULATIONS

C. A. Wemple (INEEL)

Expansion of the particle transport code rtt_MC was initiated to include neutron energies up to 100 MeV (ultra-fast region). This expansion consists of several separate phases: (1) cross section acquisition, processing and formatting; (2) development of ultra-fast neutron tracking routines; (3) development of proton (hydrogen) recoil dose computation routines; and (4) development of ultra-fast photon-production routines. The first three phases have been completed, and work is in progress on phase 4.

Ultra-fast neutron and photon production cross sections were acquired from Los Alamos National Laboratory, XTM division, in MCNP (Monte Carlo N-particle) format[1]. This set included nine nuclides - beryllium, carbon, oxygen, aluminum, silicon, calcium, iron, tungsten, and $^{238}U$. Two additional nuclides, hydrogen and nitrogen, were acquired from the National Nuclear Data Center at BNL[2], and processed locally into MCNP format using the NJOY[3] code. All these cross sections were based on updated ENDF/B-VI evaluations[2]. A modified MCNP format was developed for use of these cross section libraries with rtt_MC.

Several new subroutines were written and added to the rtt_MC code to perform the neutron tracking in the ultra-fast energy region. These routines roughly parallel the existing tracking routines for lower energy neutrons. Additional subroutines analyze the ultra-fast neutron scattering, according to the scattering laws provided in the ultra-fast cross section libraries.

Subroutines have been written to perform recoil proton tracking for computation of the proton recoil dose from scattering of neutrons on hydrogenous materials. These routines utilize a simple, straight-line slowing down approximation to determine the energy deposited by the protons along their flight path. This flight path is determined by the kinematics of neutron scattering on hydrogen, and is not changed during the slowing down. Tallies of the energy deposited are performed by edit voxel, in a similar fashion to other tallies in rtt_MC. This capability has not yet been fully implemented in the production versions of rtt_MC, but work is progressing in this area.

## REFERENCES

1. R. C. Little, *Summary Documentation for the 100XS Neutron Cross Section Library (Release 1.0),* XTM:95-259, Los Alamos National Laboratory, October 1995.

2. P. F. Rose and C. L Dunford, ed., *Data Formats and Procedures for the Evaluated Nuclear Data File, ENDF-6,* BNL-NCS-44945 (ENDF-102), Brookhaven National Laboratory, July 1990.

3. R. E. MacFarlane and D. W. Muir, *The NJOY Nuclear Data Processing System Version 91,* LA-12740-M, Los Alamos National Laboratory, October 1994.

# COLLABORATIVE SPECTRAL CHARACTERIZATION OF THE FINNISH EPITHERMAL-NEUTRON BEAM FACILITY FOR BNCT

**D. W. Nigg, Y. D. Harker, J. K. Hartwell, and C. A. Wemple (INEEL)**

**T. Seppälä (Department of Physics, University of Helsinki)**

**T. Serén, K. Kaita, I. Auterinen (Technical Research Centre of Finland)**

## INTRODUCTION

The Technical Research Centre of Finland (Valtion Teknillinen Tutkimuskeskus, or VTT) has constructed an advanced epithermal-neutron beam facility for use in BNCT research[1-3]. This facility is located at the TRIGA research reactor FiR1 in Otaniemi, near Helsinki, and was brought into initial full-power operation in April, 1996. As part of a long-standing and very productive BNCT collaboration that has existed between VTT and the INEEL, the INEEL was invited to participate in the first experimental characterization of the neutron output produced by this important new facility. This report summarizes the results of a series of collaborative measurements and computations performed by the INEEL/VTT team in connection with this effort, which began in May, 1996 with an on-site experimental campaign, followed by data reduction efforts extending through the end of 1996. It may be noted that, in addition to the work reported here, the VTT team performed some independent spectral characterization measurements during the same time period. These are reported separately[3]. In addition, a team from the Nuclear Research Institute of the Czech Republic also performed some beam measurements during the same time period. Figure 3 shows the Finnish, American, and Czech participants in the overall international FiR1 beam characterization effort.

## FACILITY DESCRIPTION

FiR1 is a standard TRIGA research reactor of the Mark-II design, produced by the General Atomics Company, La Jolla, California, USA. The reactor core, surrounded by a graphite reflector, is at the bottom of a heavily-shielded, light-water-filled concrete tank. There is a standard large graphite-filled thermal column access port on one side of the shield tank providing direct access to the source of neutrons leaking from the adjacent side of the reactor core. Figure 4 shows the shield tank and the thermal column access port with the thermal column shield plug in place. This shield plug can be pulled back on steel rails to provide access to the graphite thermal column itself.

Figure 5, taken from Reference 1, shows the basic structure of the modifications made to the FiR1 facility to produce an epithermal-neutron source for BNCT. The graphite in the thermal column region was replaced with a unique filtering and moderating material especially developed by VTT for the purpose (Trademark FLUENTAL). This material is composed of aluminum fluoride ($AlF_3$), elemental aluminum, and natural-abundance lithium fluoride (LiF), in the approximate proportions of 69%, 30%, and 1% by weight, respectively. It is prepared by hot isostatic pressing of a uniform fine-grain mixture of the components to produce a solid, chemically- and mechanically-stable composite material having a density of approximately 3 g/cm$^3$. The resulting material is quite easy to handle and it has excellent neutronic properties. Fission neutrons leaking from the TRIGA core and passing through this material are filtered and moderated in a manner that produces a near-optimal epithermal-neutron spectrum (neutrons in the 0.5 eV to 10 keV energy range) on the downstream side, with a very low level of contamination by undesirable fast neutrons

(neutrons having energies above 10 keV). The filtering and moderating region is approximately 75 cm thick along the beam axis and is followed by a bismuth gamma shield having a thickness of approximately 9 cm, as shown in Figure 5. A conical beam collimator structure extending out from the downstream face of the bismuth gamma shield was installed in September, 1996, but all measurements and calculations presented here are for the beam flux produced directly adjacent to the downstream side of the bismuth shield, with no collimator.

Figure 6 shows the temporary shielding placed around the thermal column access port during the operations for which results are reported here. Ultimately, a heavily-shielded patient treatment room will be constructed in this area. Figure 7 is a view upstream into the thermal column access port, showing the bismuth beam face, which was covered by a lithiated-polyethylene beam delimiter with a large (50 cm by 50 cm) square aperture. Further temporary shielding of the space immediately adjacent to, and downstream of, the bismuth beam face was provided by a cubical enclosure constructed of borated polyethylene blocks in the ceiling and boric-acid-filled polyethylene tiles on the walls and on the floor as shown (the downstream cover of this enclosure was removed in Figure 7). Finally, during reactor operation, the movable concrete shield plug was rolled into place to seal off the entire thermal column access port, yielding acceptably-low occupational radiation levels in the immediately-adjacent area at all times.

## METHODS AND MATERIALS

Computations and corresponding measurements of the neutron spectrum produced at the bismuth beam face were performed using techniques that have been adapted for BNCT applications by the INEEL as a result of experience with other epithermal-neutron facilities in the U.S. and in Europe. The various methods are described in the following sections.

### Theoretical Computations

The expected neutronic performance of the FiR1 epithermal-neutron beam facility was computed by VTT using the two-dimensional discrete-ordinates method as implemented in the well-known DORT[4] code, with a cross section library prepared largely from basic data available on the 67-group coupled (47 neutron groups, 20 gamma groups) BUGLE-80 library[5]. Supplementary cross section data for bismuth were provided by INEEL for use in the calculation. The entire reactor-moderator system was modeled in cylindrical (R-Z) geometry. The Z-axis in the DORT calculation was aligned with the physical beam centerline and a symmetric $S_8$ quadrature set was employed. Use of this type of two-dimensional approximation requires that the reactor core be rather creatively modeled as a cylinder on its side, but experience[6,7] has shown that this modeling assumption can produce remarkably accurate results, both in comparison with measurement as well as in comparison with exact-geometry MCNP[8] Monte Carlo calculations, as long as certain key dimensions and component volumes are preserved. Although the original design calculations for the FiR1 beam were accomplished by VTT using three-dimensional discrete-ordinates computations[1,2], the need for greater detail in the present work, as well as the need to perform a very large number of computations for various experimental conditions dictated that the much more computationally-efficient two-dimensional approximation be used for all work reported here.

The basic DORT computational model for the reactor-moderator system was constructed by VTT in two parts, following previous practice at INEEL. A "core" model which included the core itself, the surrounding graphite reflector and immediately-adjacent water, as well as the first 20 centimeters of the moderator region was first used to compute the leakage spectrum of core neutrons into the moderator. This was an eigenvalue-type calculation. As mentioned previously, some rather severe modeling approximations were necessary to represent the

core and the surrounding graphite reflector in this model. Details of the model will not be reported here. Basically, the various regions of the non-uniformly-loaded core were approximately represented, as were the regions of the surrounding reflector. Thickness of the regions along the extended beam centerline axis were preserved and the radii were allowed to vary in the model to preserve appropriate region volumes. A so-called "internal boundary source" file containing the angular fluxes at the axial location corresponding to the beginning of the moderator region was saved for use as a fixed-flux boundary condition in a subsequent DORT "moderator" model that represented the entire moderator region out to, and beyond, the bismuth shield face where the measurements were taken. As mentioned, the "core" model also included the first part of the moderator to account for the backscattering effect of the moderator on the flux at the location where the boundary source was taken. The "core" model was used only to compute the leakage of neutrons from the TRIGA core into the moderator region. Criticality of the core model was achieved by artificial manipulation of the modeled boron concentration in the control rod regions to produce a calculated eigenvalue of unity.

The DORT "moderator" model uses the leakage source from the core model on its upstream side and simply computes the resulting filtered and moderated flux existing at the bismuth face, at the measurement point on the downstream side. This model is much more geometrically-realistic a-priori, since the moderator region does have a relatively high degree of cylindrical symmetry about the beam centerline axis. The calculation performed with the moderator model is thus of the fixed-source type. It is very computationally-efficient and can be run repeatedly for a wide variety of downstream moderator configurations and measurement apparatus arrangements without having to rerun the time-consuming core calculation, as long as the part of the moderator immediately adjacent to the core and graphite reflector is not significantly changed.

**Activation Foil Measurements**

Measurements of the intensity and spectrum produced at the bismuth gamma shield face of the FiR1 moderator assembly were performed using activation-foil techniques[9], supplemented by some limited proton-recoil measurements. The activation-foil techniques will be described in this section, followed by a description of the proton-recoil techniques in the next section.

The foil materials and neutron interactions that were used in the measurements performed by the INEEL team are listed in Table 1. All foils had a thickness in the range of 0.0254 mm to 0.127 mm and were arranged in stacks of five, with a cadmium cover surrounding each package of five foils to suppress the responses of the foils to thermal neutrons. In addition to these foils, small gold wires (diameter 0.254 mm), with and without cadmium covers, were provided by VTT for use in the measurements. The six sets of foils were positioned in a so-called "foil wheel", machined from an aluminum disk by INEEL especially for this type of measurement. This foil wheel is shown in Figure 8. Reproducible positioning of the foil wheel on the beam axis at the bismuth face of the FiR1 moderator assembly was accomplished using a simple device made from a corrugated cardboard sheet with an appropriate cutout as shown in Figure 9.

To provide additional spectral information in the high-energy range, indium and copper foils were also placed in a small hollow boron-10 sphere during some irradiations. The inside diameter of the boron sphere was approximately 2.5 cm. The outside diameter was approximately 5 cm. The positioning of the boron sphere during irradiation is shown in Figure 10. During the irradiations involving the boron sphere the VTT cadmium-covered and bare gold wires were placed in azimuthally- symmetric locations just below the boron sphere (but far enough below and to each side of the sphere to be away from the flux perturbation caused by the sphere).

**Table 1.** Activation interactions used in the INEEL FiR1 epithermal-neutron beam measurements.

| Interaction | Energy Range of Primary Response | Activation Gamma Energy of Interest (keV) |
|---|---|---|
| $^{115}$In (n,γ) | 1 eV Resonance | 1293, 1097, and 416 |
| $^{115}$In (n,n') | 430 keV Threshold | 336 |
| $^{197}$Au (n,γ) | 5 eV Resonance | 411 |
| $^{186}$W (n,γ) | 18 eV Resonance | 686 |
| $^{59}$Co (n,γ) | 132 eV Resonance | 1173 |
| $^{55}$Mn (n,γ) | 340 eV Resonance | 847 |
| $^{63}$Cu (n,γ) | 1 keV Resonance | 511 (Positron) |

Use of the foils and wires as described provided nine basic neutron response functions having a useful degree of linear independence for use in a direct spectral unfolding process. These were: resonance absorption in the copper, manganese, cobalt, tungsten, and indium foils in the spectrum wheel, all with thermal absorption suppressed by cadmium; resonance-neutron and thermal-neutron absorption in the covered and uncovered gold wires, and finally; inelastic scatter in the indium foils in the boron sphere as well as resonance absorption in the indium foils in the boron sphere, with heavy suppression of thermal and epithermal flux due to the presence of the boron sphere. Resonance absorption in the copper foils within the boron sphere was also available, but was not used in the full-range spectrum unfolding process due to insufficient linear independence of the response function. Gold foils were also irradiated in the spectrum wheel, but the wire data were used for the full-range unfolding results reported here.

As noted, the foils irradiated in the spectrum wheel were in stacks, with each package containing five foils of the same material, one package for each material used in the spectrum wheel. The first foils in each stack (i.e. closest to the bismuth face) were used for the primary spectrum unfolding process. However it may be noted that at the center foils (designated as foil number three in each stack) also record useful spectral information, since these foils are shielded from neutrons at the resonance energy of each foil material. These center foils were used to obtain additional pointwise spectral information as will be described. The foils irradiated in the boron sphere were in stacks of four, but the responses of all four foils were combined to provide better counting statistics for the activity induced in these foils. Information from the separate foils within in the boron sphere was not used.

Unshielded and effective shielded cross sections, relative a-priori reaction rates, and a-priori neutron fluxes for all foils in the various packages as well as for the gold wires were computed using MCNP models of the various dosimeter packages. The MCNP models for each stacked-foil package and for the two gold wires were very simple. The neutron source for each MCNP model was based on a representation of the plane source emerging from the downstream side of the final bismuth gamma shield. The information for this source was constructed using calculated results from the DORT "moderator" model. Each dosimeter package (foils or wire), with surrounding cadmium as appropriate, was then modeled adjacent to the source plane. The calculated cross sections (reaction rate divided by flux) for each interaction of interest in each region of each dosimeter package were coalesced to 9 energy groups, with the 9-group energy boundaries determined by the energy ranges of maximum sensitivity associated with each of the nine basic linearly-independent dosimeter response functions

defined previously. These were then used in a direct coarse-group spectral unfolding process involving the solution of a 9x9 system of linear equations describing the dosimeter reaction rates and fluxes in the usual manner. Least-squares adjustment techniques were not used by INEEL for the preliminary measurements reported here, although such techniques were used by the VTT team[3] with very consistent results, as will be described later.

The measurements reported here are based on the results of four full-power (250 kW) FiR1 irradiations, two for the foil packages in the spectrum wheel and two for the sets of foils in the boron sphere. The gold wires were irradiated during the same irradiation as the boron sphere foils. The induced activities of all foils and wires were measured by VTT using standard calibrated gamma spectroscopy instrumentation (germanium detector with appropriate electronics, PC-based spectral analysis hardware and software, etc.) that was available at the VTT facility. All foil and wire activity results were reported by VTT to the INEEL team and subsequent analysis was carried out by the INEEL team using PC-based software developed especially for the purpose. This latter software corrected the measured foil activities for decay time, irradiation time, detector efficiency, branch ratios and so forth to produce measured foil activation rates per atom of activated material. Following this process the specified system of activation equations was solved to produce coarse-group scalar neutron fluxes at the bismuth face corresponding to the measured activation rates, corrected for self-shielding in each foil. These fluxes could then be directly compared to corresponding theoretical fluxes at the measurement location, calculated by VTT using the DORT moderator model.

**Proton-Recoil Measurements**

A series of proton recoil measurements was also performed on the beam, again at the location of the bismuth shield face. The measurement apparatus is shown in Figure 11. The detector was a 2.38 cm diameter by 7.62 cm active length proportional counter tube (manufactured by Reactor Controls, Inc.) filled with hydrogen at a pressure of 200 cm (Hg), 10 cm (Hg) methane, and 10 cm (Hg) nitrogen. The analog electronics included a Canberra 3002D High Voltage Power Supply, an Ortec 142PC preamplifier, and an Ortec 570 Linear Amplifier (3 microsecond semi-Gaussian shaping). The amplified and shaped pulses were digitized by a Nuclear Data 579 successive approximation Analog-to-Digital converter (ADC). The ND 579 ADC was interfaced to a Canberra AccuSpec Acquisition Interface Board that occupied a slot in a 386-based personal computer. Acquisition control and display functions, along with certain rudimentary calculations (for example, energy calibration), were performed through the personal computer using Canberra's AccuSpec Data Acquisition and Control Software (Version 7.3). The high voltage power supply (HVPS) was set to +2,180V and the amplifier gain set to a total gain of X10. With an ADC conversion gain of 512 channels, these settings gave an energy calibration of 4.055 keV/channel and a maximum storage energy of greater than 2,000 keV, well beyond the linear range of the tube.

The presence of a large thermal-neutron component in the measurement environment complicated measurements with the apparatus as described. The proton peak produced from the thermal neutron (n,p) reaction in N-14 was large, and compromised the spectral data in the region from about 500 keV to about 750 keV. The upper tube limit is about 1 MeV. To decrease this thermal component, the proportional counter was wrapped with 0.4 mm of Cd, and for at least one run was surrounded on 5 sides with 2 cm of borated polyethylene. Still the large thermal peak persisted. The spectral data were analyzed both with a version of the PSNS spectral unfolding code[10] and using the HEPRO suite of unfolding codes[10]. The HEPRO unfolding used response functions generated by the Monte Carlo code GNSR[12]. Both analysis approaches gave similar results. The Czech team performed parallel measurements with plastic proton-recoil detectors. The results will be reported separately.

## RESULTS

Table 2 shows the final un-normalized foil interaction rates for each of the four reactor runs where INEEL dosimeters were activated. This information is uncorrected for the slightly different reactor powers encountered in each of the runs, and the boron sphere foil data are uncorrected for the slight divergence of the free beam over the 2.5 cm distance between the bismuth face and the foil location within the sphere. Auxiliary measurements made by the Czech team, as well as theoretical calculations both indicate that the divergence effect is 5% or less, due to the large lateral extent of the bismuth face.

Table 3 shows the final combined, re-normalized, foil interaction rates that were used in the unfolding process. Data for Runs 1 and 3 (spectrum wheel foils) were combined, as were data from Runs 2 and 4 (boron sphere foils). This was done by fluence-weighting the Table 2 data to combine the rates for the two separate runs in each case, and then re-normalizing the resulting combined activation rate for each foil to an effective power of 250 kW. The data for the gold wire were simply re-normalized to 250 kW, since this experiment was not repeated. The reactor energy releases and run times used for the above process were as follows:

Run 1 (5/15/96): Energy Release 230 kW-hr, Run Time 60 minutes.
Run 2 (5/16/96): Energy Release 249 kW-hr, Run Time 60 minutes.
Run 3 (5/16/96): Energy Release 525 kW-hr, Run Time 127 minutes.
Run 4 (5/20/96): Energy Release 266 kW-hr, Run Time 65 minutes.

Figure 12 shows a directly-unfolded free-field unperturbed spectrum obtained from the full 9x9 system of equations describing the foil activation rates. Elements of the unfolding matrix were computed within appropriate energy ranges using MCNP for (in order of increasing primary energy of response): the uncovered gold wire, the cadmium-covered indium foil in the spectrum wheel at the top of the stack (Foil 1, nearest the bismuth face), the covered gold wire, the first covered tungsten, cobalt, manganese, and copper foils in the spectrum wheel, and finally, the covered indium foil in the boron sphere (capture and inelastic scatter activation rates were taken as separate responses). The corresponding measured reaction rates for the same foils were used as the source terms in the 9x9 system. As mentioned previously, the copper foil in the boron sphere did not have a response function that was sufficiently linearly-independent from that of the indium foil in the sphere to add any information so it was not included in this particular unfolding calculation. Also included in Figure 12 for comparison is the computed spectrum at the bismuth face, based on the discrete-ordinates calculations, normalized to a core power of 250 kW. It may be noted that agreement of the calculated and measured spectrum is quite good, especially in the epithermal-neutron range. The measured thermal neutron flux (energy below 0.5 eV) is substantially larger than calculated, however, but this was not unexpected, given the nature of the beam configuration as it existed for these measurements. The hydrogenous materials in the vicinity of the bismuth face contribute to the thermal neutron environment. These materials were represented as well as possible in the computational model, but the nature of the model did not allow a complete treatment. As noted, the final configuration of the FiR1 beam includes a neutron-absorbing collimator as well as other features designed to suppress this unwanted thermal flux component at the patient location.

Figure 13 shows an unfolded spectrum obtained by a somewhat different and to some extent, independent, method. In this case, flux values for various neutron energies of interest were computed using the measured data from the different dosimeter materials individually rather than in a full-range coupled system of equations. The average measured neutron flux in the thermal energy range (0.001 eV to 0.5 eV) was estimated using the covered and uncovered gold wire data. A system of two equations in two unknowns, where the first variable was the total energy-integrated flux above 0.5 eV and the second variable was the total flux below 0.5 eV was constructed and solved using the measured

**Table 2.** Un-normalized FiR1 Dosimeter Activation Rates (reactions/atom-sec)

| Spectrum Wheel Irradiations | Energy of Primary Activation Gamma | Run 1 (5/15/96) | Run 3 (5/16/96) |
|---|---|---|---|
| $^{63}Cu$ (n,γ) | | | |
| Foil 1 | 511 keV | 4.34 E-16 | 4.28 E-16 |
| Foil 3 | 511 keV | 3.20 E-16 | 3.11 E-16 |
| $^{55}Mn$ (n,γ) | | | |
| Foil 1 | 847 keV | 1.73 E-15 | 1.68 E-15 |
| Foil 3 | 847 keV | 1.19 E-15 | 1.16 E-15 |
| $^{59}Co$ (n,γ) | | | |
| Foil 1 | 1173 keV | 8.16 E-15 | 7.87 E-15 |
| Foil 3 | 1173 keV | 4.42 E-15 | 4.26 E-15 |
| $^{186}W$ (n,γ) | | | |
| Foil 1 | 686 keV | 6.31 E-14 | 6.00 E-14 |
| Foil 3 | 686 keV | 2.54 E-14 | 2.51 E-14 |
| $^{197}Au$ (n,γ) | | | |
| Foil 1 | 411 keV | 8.55 E-14 | 8.18 E-14 |
| Foil 3 | 411 keV | 3.34 E-14 | 3.17 E-14 |
| $^{115}In$ (n,γ) | | | |
| Foil 1 | 416 keV | 1.08 E-13 | 1.06 E-13 |
| Foil 3 | 416 keV | 3.95 E-14 | 4.00 E-14 |
| Foil 1 | 1097 keV | 1.06 E-13 | 1.03 E-13 |
| Foil 3 | 1097 keV | 3.86 E-14 | 3.89 E-14 |
| Foil 1 | 1293 keV | 1.06 E-13 | 1.03 E-13 |
| Foil 3 | 1293 keV | 3.86 E-14 | 3.89 E-14 |

| Boron Sphere Irradiations | Energy of Primary Activation Gamma | Run 2 (5/16/96) | Run 4 (5/20/96) |
|---|---|---|---|
| $^{115}In$ (n,n') | | | |
| 4 Foils | 336 keV | 3.74 E-19 | 3.25 E-19 |
| $^{115}In$ (n,γ) | | | |
| 4 Foils | 416 keV | 6.55 E-17 | 5.70 E-17 |
| $^{63}Cu$ (n,γ) | | | |
| 1 Foil | 511 keV | 1.50 E-17 | 1.53 E-17 |

| VTT Gold Wire Irradiations | Energy of Primary Activation Gamma | | Run 4 (5/20/96) |
|---|---|---|---|
| $^{197}Au$ (n,γ) | | | |
| Cd Cover | 411 keV | | 4.24 E-14 |
| No Cd Cover | 411 keV | | 6.22 E-14 |

**Table 3.** Combined and Re-normalized FiR1 Dosimeter Activation Rates (reactions/atom-second) at 250 kW.

| Spectrum Wheel Irradiations | Energy of Primary Activation Gamma | Combined and Re-normalized FiR1 Dosimeter Activation Rates |
|---|---|---|
| $^{63}Cu$ (n,γ) | | |
| Foil 1 | 511 keV | 4.49 E-16 |
| Foil 3 | 511 keV | 3.27 E-16 |
| $^{55}Mn$ (n,γ) | | |
| Foil 1 | 847 keV | 1.77 E-15 |
| Foil 3 | 847 keV | 1.22 E-15 |
| $^{59}Co$ (n,γ) | | |
| Foil 1 | 1173 keV | 8.30 E-15 |
| Foil 3 | 1173 keV | 4.49 E-15 |
| $^{186}W$ (n,γ) | | |
| Foil 1 | 686 keV | 6.36 E-14 |
| Foil 3 | 686 keV | 2.63 E-14 |
| $^{197}Au$ (n,γ) | | |
| Foil 1 | 411 keV | 8.64 E-14 |
| Foil 3 | 411 keV | 3.36 E-14 |
| $^{115}In$ (n,γ) | | |
| Foil 1 | 416 keV | 1.11 E-13 |
| Foil 3 | 416 keV | 4.15 E-14 |
| Foil 1 | 1097 keV | 1.08 E-13 |
| Foil 3 | 1097 keV | 4.05 E-14 |
| Foil 1 | 1293 keV | 1.08 E-13 |
| Foil 3 | 1293 keV | 4.05 E-14 |

| Boron Sphere Irradiations | Energy of Primary Activation Gamma | Combined and Re-normalized FiR1 Dosimeter Activation Rates |
|---|---|---|
| $^{115}In$ (n,n') | | |
| 4 Foils | 336 keV | 3.53 E-19 |
| $^{115}In$ (n,γ) | | |
| 4 Foils | 416 keV | 6.18 E-17 |
| $^{63}Cu$ (n,γ) | | |
| 1 Foil | 511 keV | 1.53 E-17 |

| VTT Gold Wire Irradiations | Energy of Primary Activation Gamma | Combined and Re-normalized FiR1 Dosimeter Activation Rates |
|---|---|---|
| $^{197}Au$ (n,γ) | | |
| Cd Cover | 411 keV | 4.32 E-14 |
| No Cd Cover | 411 keV | 6.33 E-14 |

reaction rates for the covered and uncovered gold wires as the source term. The resulting thermal flux per unit lethargy is shown by the solid circles in Figure 13, with the line between the circles representing the energy range over which the average flux applies.

The next six pointwise values in Figure 13 (shown as solid triangles) were obtained using the first and third foils in each of the six stacked foil packages in the aluminum spectrum wheel. A system of two equations in two unknowns was constructed for each foil type. The first unknown was the energy-integrated flux within a narrow energy group centered on the primary resonance for the foil material of interest. The second unknown was the total neutron flux integrated over all energies outside of the narrow resonance group, both above and below. The source term was then constructed using the measured reaction rates in the first and the third foil in the foil stack. The response function of the third foil in a given stack is linearly-independent from the response function of the first foil in the stack due to the suppression of the resonance flux in the third foil relative to that in the first foil. Solution of the resulting 2x2 system of equations then gives the total flux in the resonance group as one element of the solution flux vector. These fluxes (per unit lethargy) are plotted in Figure 13. They were obtained using the response data from, in order of increasing primary resonance energy, the indium, gold, tungsten, cobalt, manganese, and copper foil stacks.

The final two flux values shown in Figure 13 were computed using the responses of the copper and indium foils that were placed within the boron sphere. The average flux in the low keV range, shown by the line between the open triangles, was obtained using the copper (n,gamma) interaction. The MCNP calculations for the copper foil in the boron sphere indicate that 99% of the total neutron capture rate occurs in the neutron energy range between 550 eV (where the primary resonance begins) and about 24 keV (near the top of the unresolved resonance range). The boron sphere effectively eliminates the sensitivity of the copper foil to neutrons below about 500 eV because of severe flux depression by the boron. The cross section itself has a low value above the unresolved energy range. Hence one can infer an average neutron flux over relatively narrow neutron energy range where the majority of the interactions occur. This is what is shown in Figure 13 for the copper foil in the boron sphere. Finally, the measured average flux in the energy range between 320 keV and about 14 MeV (above which there are essentially no fission source neutrons) is shown by the line between the two open circles in Figure 13. This was obtained in the standard manner using the measured inelastic scatter interaction rate in the indium foil within the boron sphere.

Integrating the measured curve shown in Figure 12 over the epithermal-neutron energy range (0.5 eV to 10 keV) yields a total epithermal flux of $1.25 \times 10^9$ neutrons per $cm^2$-s at 250 kW. Integration of the calculated theoretical spectrum over the same energy range yields an expected epithermal flux of about $1.1 \times 10^9$ $n/cm^2$-s at 250 kW. Thus the beam appears to be producing a slightly higher epithermal-neutron flux than expected from the discrete-ordinates calculations, but still in good agreement for preliminary survey measurements of this type, given the uncertainties inherent in the calculational approximations that were used as well as the uncertainties of the measurements, which are estimated to be approximately 8% (1 sigma) in the epithermal energy range, including the measurement uncertainties as well as the computational uncertainties associated with the diagonal elements of the unfolding matrix. (The matrix was well-conditioned, and the uncertainty in the off-diagonal elements did not appear to significantly affect the results).

Integrating the measured curve shown in Figure 12 from 10 keV to the top of the energy range yields a total fast neutron flux value of $4.35 \times 10^7$ $n/cm^2$-s at 250 kW, with an estimated uncertainty of approximately 15% (1 sigma) from all sources. Integration of the calculated spectrum yields a fast flux of $1.98 \times 10^7$ $n/cm^2$-s. This is somewhat lower than measured, but not inconsistent with previous experience[6] in connection with the BNL epithermal-neutron beam. The group structure of the BUGLE-80 library is somewhat coarse in

some parts of the fast neutron energy range, and neutron streaming through cross section minima can be understated in the calculations.

A simple, but widely-used metric for the quality of reactor-based epithermal-neutron beams is based on dividing the free-field neutron KERMA rate of the beam (integrated over all energies above thermal) by the useful epithermal-neutron flux, again measured in the free field. The results of the DORT calculations are first used to estimate spectrum-averaged neutron kerma factors for the fast and epithermal components of the FiR1 beam. These can then be applied to the measured fast and epithermal fluxes to compute the total neutron dose in the free field. Dividing this by the useful epithermal flux then yields a measured estimate of $2.0 \times 10^{-11}$ cGy total neutron dose per unit useful epithermal-neutron flux, within the expected range of agreement with the DORT calculations (which yielded a value of $1.26 \times 10^{-11}$ cGy per unit flux) as well as with the results of earlier three-dimensional beam design calculations performed by VTT[1,2]. When evaluated on the basis of this metric, the FiR1 epithermal neutron beam has the highest spectral quality of the four currently-operating reactor-based epithermal-neutron beams worldwide.

Finally, a single point representing the best-estimate results of the proton-recoil measurements in the energy range between 200 and 400 keV is also shown in Figure 13. As noted, the high thermal-neutron flux component at the measurement location compromised the proton recoil results above about 500 keV. Hence, only the results below this energy range are presented here. The value shown is a single average flux over the 200-400 keV energy range, at 250 kW reactor power, unfolded using the PSNS[10] code. The numerical value is $1.53 \times 10^{6}$ n/cm$^2$-sec, with an uncertainty of approximately 20% (1 sigma), in reasonable agreement with the results obtained from the foil measurement based on inelastic scattering in indium.

## DISCUSSION

The INEEL has had a strong historical interest in the use of the VTT aluminum fluoride based epithermal neutron moderating material for applications involving new reactor-based and accelerator-based epithermal-neutron sources for BNCT[13,14]. The opportunity to experimentally confirm the expected neutronic performance of this material in an actual reactor application has been quite valuable. Additional confirmation of the performance was also demonstrated by the various contemporaneous measurements made separately by the VTT team[3]. For instance, Reference 3 quotes measured values of $1.26 \times 10^{9}$ n/cm$^2$-sec and $2.63 \times 10^{7}$ n/cm$^2$-sec for the epithermal and fast fluxes, with uncertainties of approximately 4% and 26%, respectively. The least-square adjustment process used to arrive at these flux values was based on reaction data from completely different dosimeter packages with sensitivities in the epithermal energy range but the indium inelastic scatter data from the INEEL foils in the boron sphere was included in the fast energy range. Thus the independently-measured epithermal flux was essentially the same as reported in the work documented in this article, and the separately-estimated fast flux was in reasonable agreement, given the known uncertainties.

Of particular note also is the fact that the work documented in Reference 3 and in this article constitutes the first experimental demonstration of the utility of small, relatively inexpensive TRIGA reactors as high-quality, clinical-scale, epithermal-neutron sources for BNCT. This is particularly significant because there are several other TRIGA reactors that could also be used for this purpose worldwide, offering the opportunity for expansion of BNCT research, which heretofore has been somewhat constrained because of the lack of suitable neutron sources in convenient geographic locations.

## REFERENCES


1. I. Auterinen and P. Hiismäki, "Design of an Epthermal-Neutron Beam for the TRIGA Reactor in Otaniemi", TKK-F-A718, Helsingin Teknillinen Korkeakoulu (Helsinki University of Technology), 1994.

2. I. Auterinen and P. Hiismäki, "Epithermal BNCT Neutron Beam Design for a TRIGA-II Reactor", In: Advances in Neutron Capture Therapy, Proceedings of the 5th International Symposium on Neutron Capture Therapy (A. Soloway and R. Barth, eds.), Plenum Press, New York, NY, 1993, pp 81-84.

3. K. Kaita, T. Serén, I. Auterinen, "Characterization of the Finnish Epithermal-Neutron Beam Using Activation Detectors", Proceedings of the 7th International Symposium on Neutron Capture Therapy, Zurich, Switzerland, September, 1996 (In publication).

4. W.A. Rhoades and R.L. Childs, "An Updated Version of the DOT-4 One- and Two-Dimensional Neutron/Photon Transport Code", ORNL-5851, Oak Ridge National Laboratory, April 1982.

5. R.W. Roussin, "BUGLE-80 Coupled 47-Neutron, 20 Gamma-Ray P3 Cross Section Library", DLC-75, Radiation Shielding Information Center, 1980.

6. F.J. Wheeler, et.al., "Epithermal Neutron Beam Design for Neutron Capture Therapy at the Power Burst Facility and the Brookhaven Medical Research Reactor", Nuclear Technology 92, 106, October, 1990.

7. D.W. Nigg, F.J. Wheeler, "Conceptual Physics Design of an Epithermal-Neutron Facility for Neutron Capture Therapy at the Georgia Tech Research Reactor", Proc. 1992 ANS Annual Meeting, Boston, MA, June 1992 (Invited).

8. "MCNP Monte Carlo Neutron and Photon Transport Code Systems", CC-200A, Radiation Shielding Information Center.

9. Y.D. Harker, et. al., "Spectral Characterization of the Epithermal-Neutron Beam at the Brookhaven Medical Research Reactor", Nucl. Sci. Eng., 110:355 (1992).

10. E.F. Bennett and T.J. Yule, "Techniques and Analyses of Fast-Reactor Neutron Spectroscopy with Proton-Recoil Proportional Counters," ANL-7763 (August 1971), Recoded in C for MS-DOS machines by Gyorgy Vizkelethy, Idaho State University.

11. M. Matzke, "Unfolding of Pulse Height Spectra: The HEPRO Program System," PTB-N-19 (October 1994).

12. M. Weyrauch, A. Casnati, and P. Schillebeeckx, "GNSR -- A Computer Code To Calculate Response Functions of Gas-Filled Neutron Detectors," PTB-N-26 (June 1996).

13. D.W. Nigg, F.J. Wheeler, "Preconceptual Performance Estimate for an Epithermal-Neutron Beam for BNCT at the GA Mark-I TRIGA Facility in La Jolla", EGG-NRE-11476, September, 1994.

14. D.W. Nigg, et. al. "Computational and Experimental Studies of an Electron Accelerator Based Epithermal Photoneutron Source Facility for Boron Neutron Capture Therapy", INEL BNCT Program 1995 Annual Report, INEL-96-0139, J.R. Venhuizen (ed.).

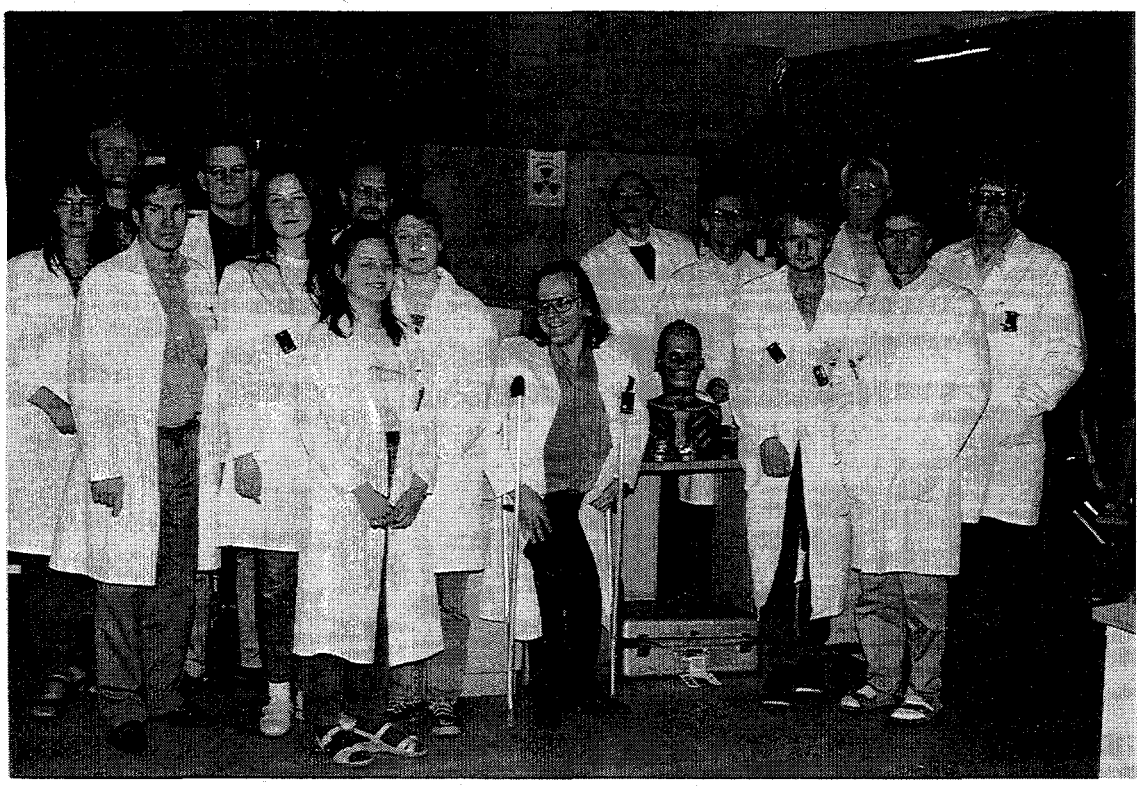

**Figure 3.** Members of the joint Finnish/Czech/U.S. FiR1 epithermal-neutron beam characterization team - Helsinki, Finland, May, 1996.

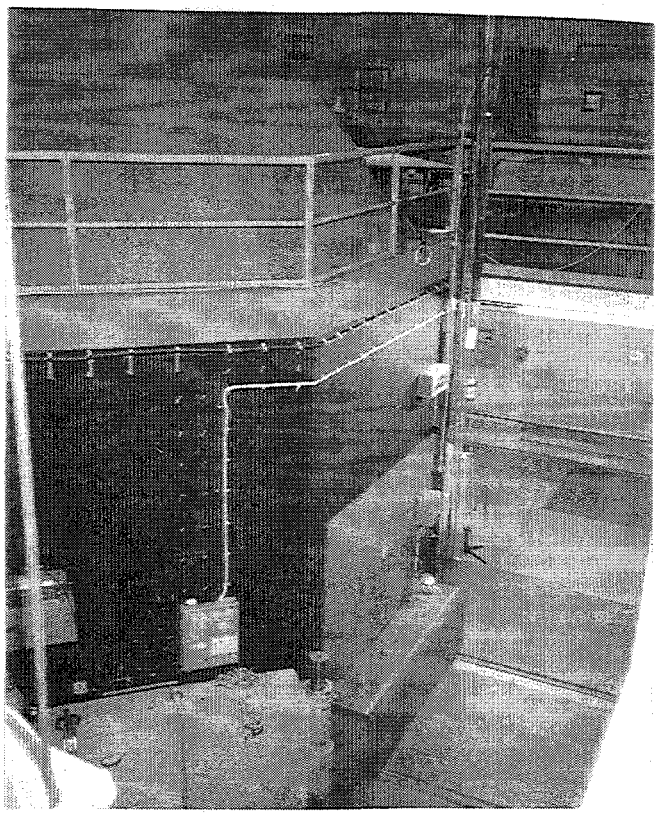

**Figure 4.** FiR1 shield tank and thermal column access port.

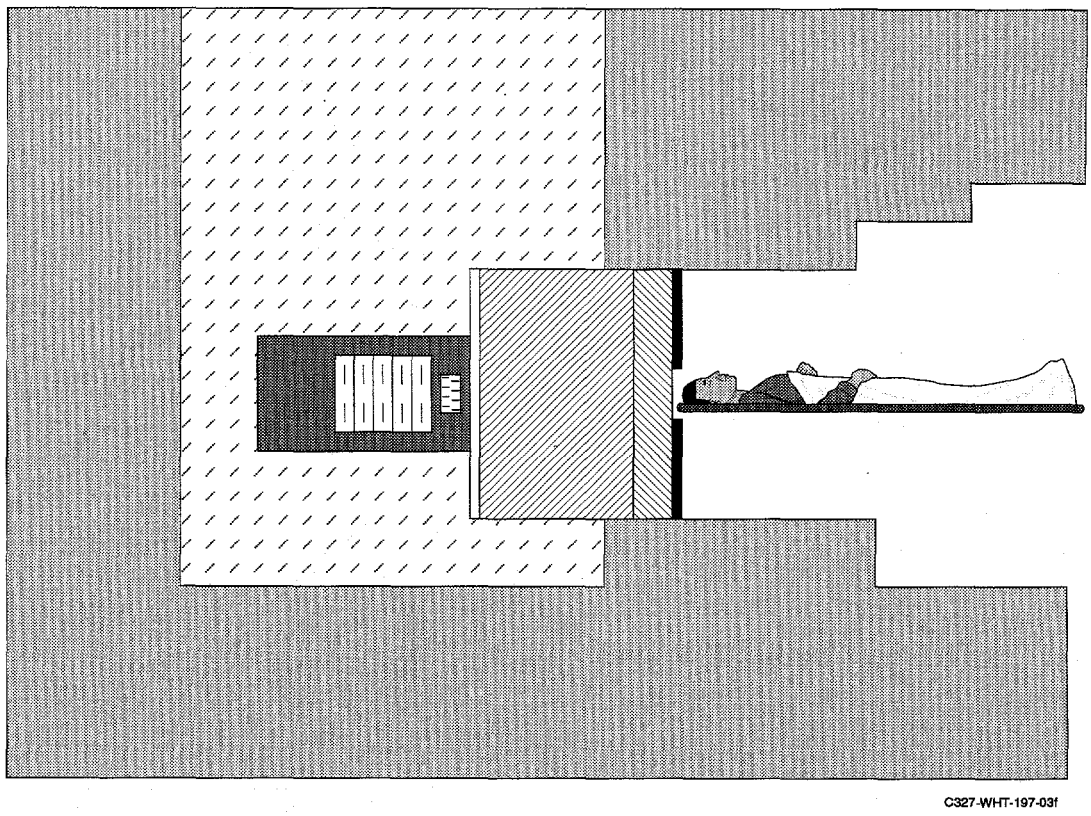


**Figure 5.** Schematic side view of the basic FiR1 epithermal beam concept.

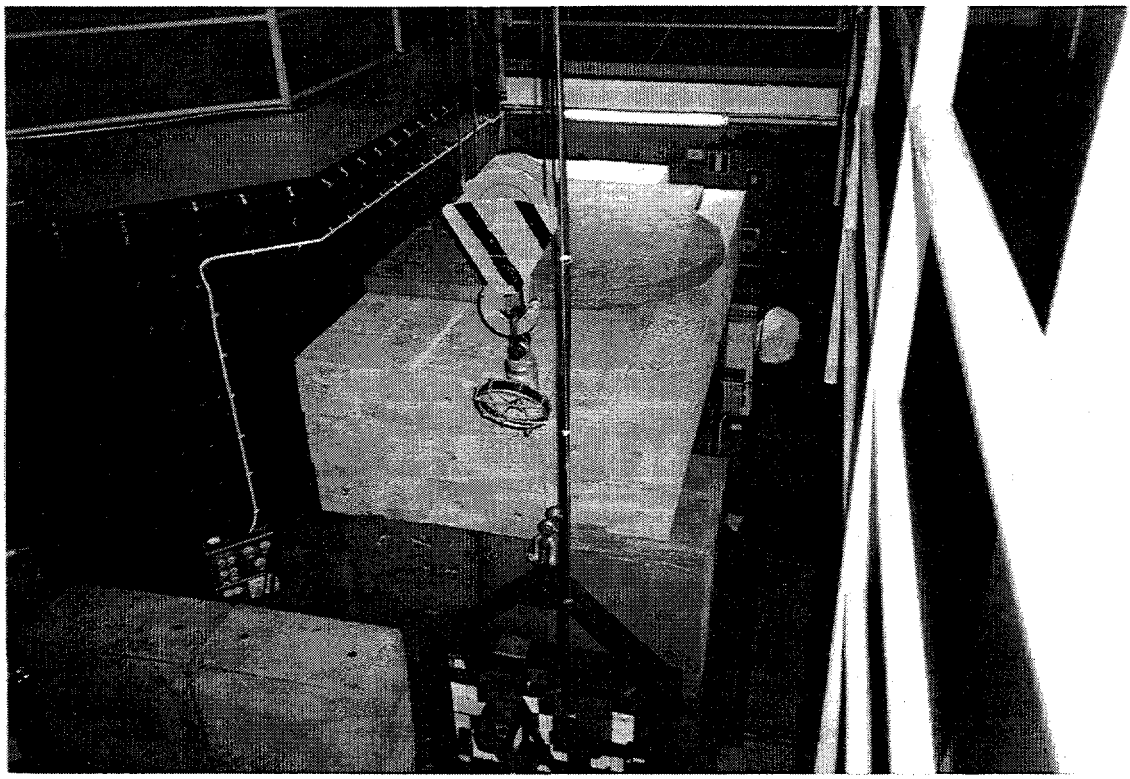

**Figure 6.** FiR1 thermal column with temporary shielding in place for BNCT measurements.

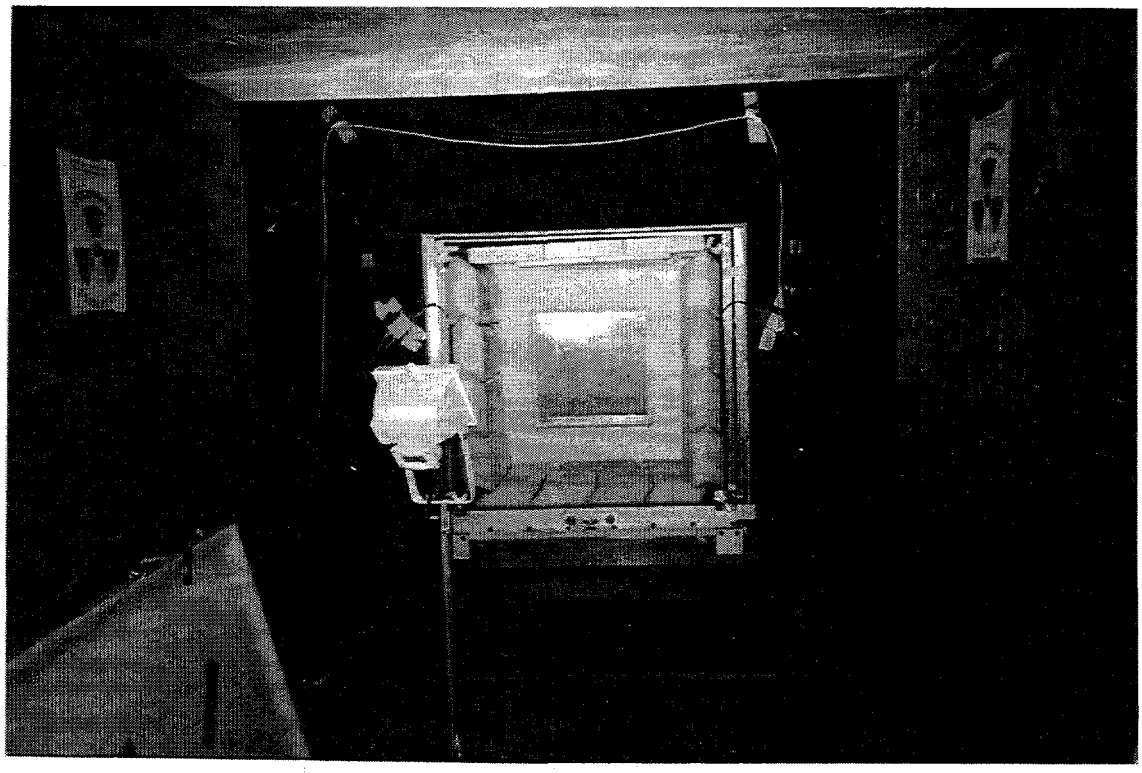

**Figure 7.** View into the FiR1 thermal column access port. The epithermal-neutron filtering and moderating assembly shown in place, followed by the bismuth shield and lithiated-polyethylene beam delimiter with a square (50x50 $cm^2$) aperture.

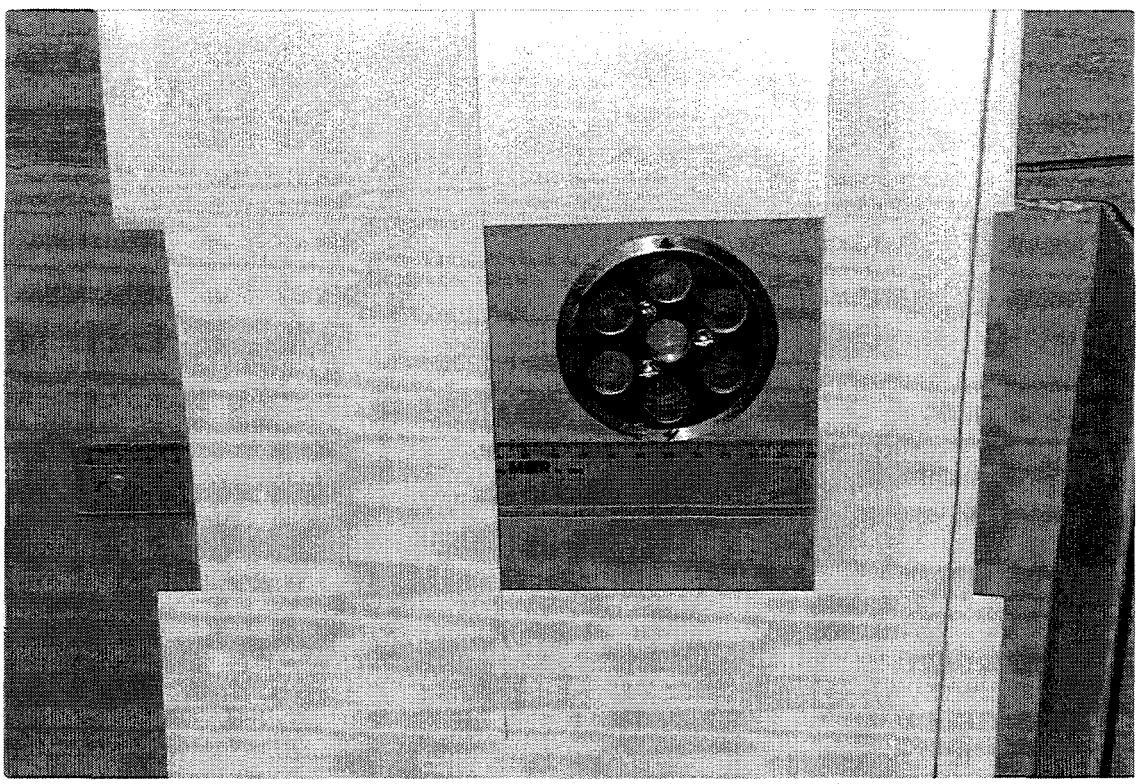

**Figure 8.** INEEL activation foil holder assembly. Dimensions are in centimeters.

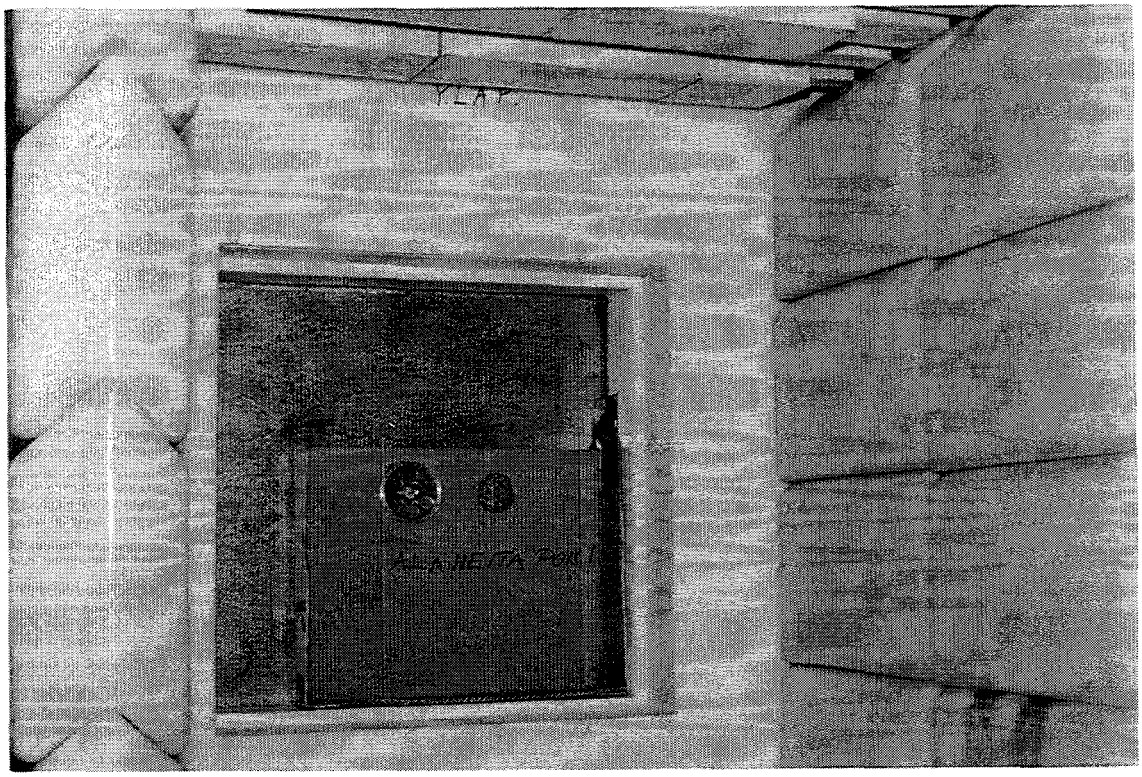

**Figure 9.** FiR1 bismuth beam face with INEEL activation foil assembly in place. The Finnish words may be translated as "Do not throw (this) away".

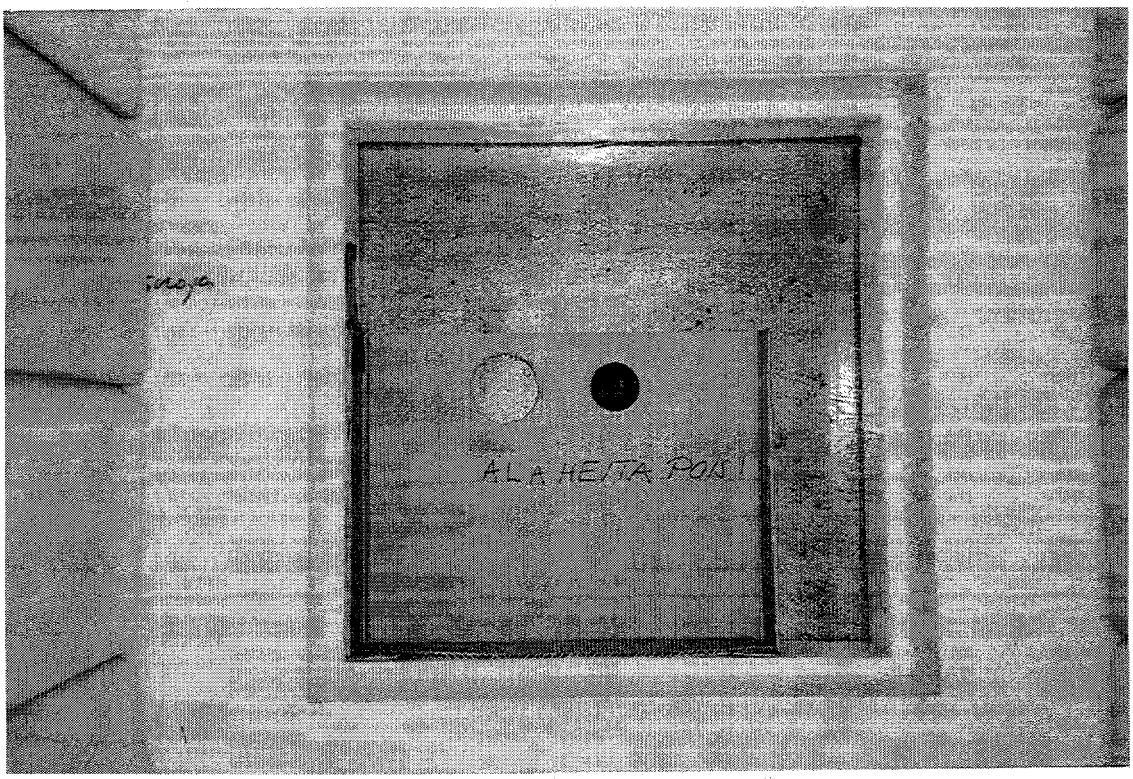

**Figure 10.** FiR1 bismuth beam face with INEEL boron sphere foil shield in place.

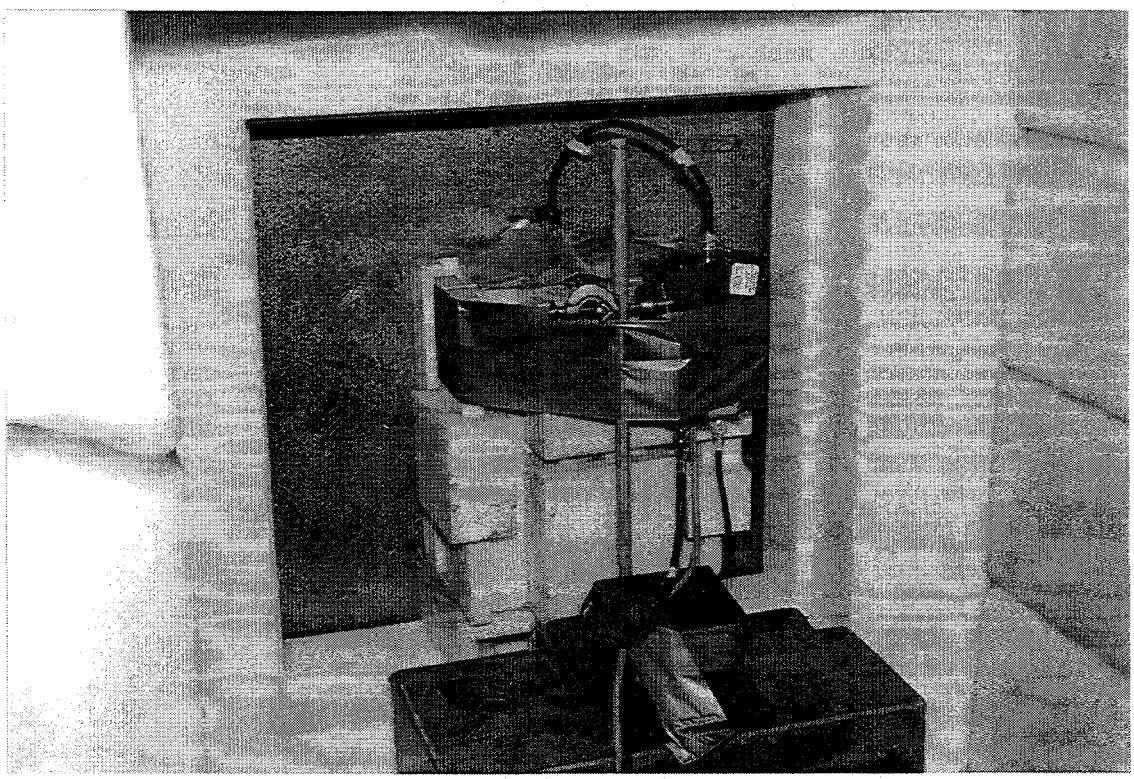

**Figure 11.** FiR1 bismuth beam face with INEEL proton-recoil apparatus in place.

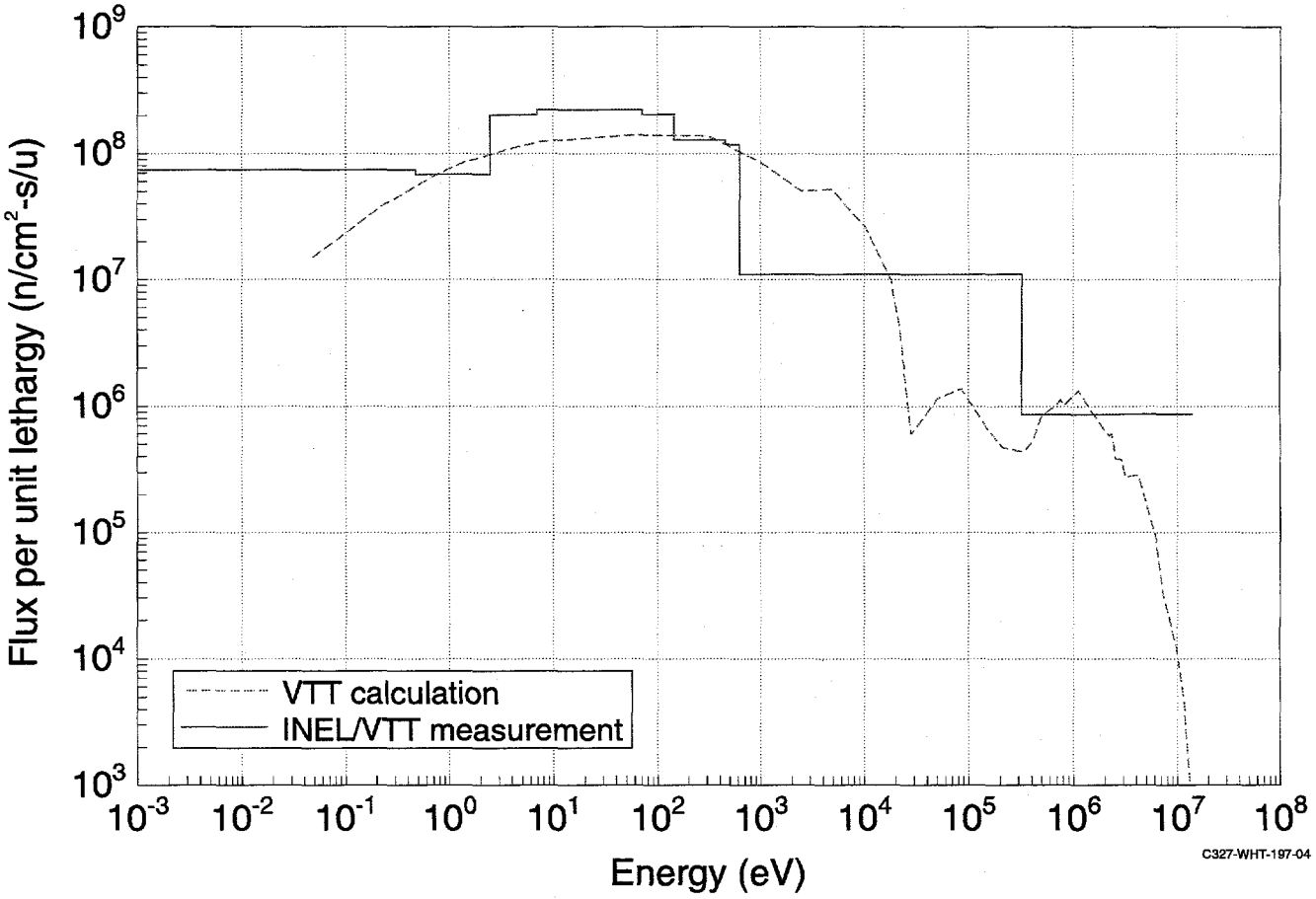


**Figure 12.** FiR1 free-beam spectrum, bismuth face, 250 kW, unfolded activation data. The measured spectral data are unfolded using a full-range direct inversion with activation data from the INEEL stacked foils (first position), the VTT gold wires, and the INEEL foils within the boron sphere.

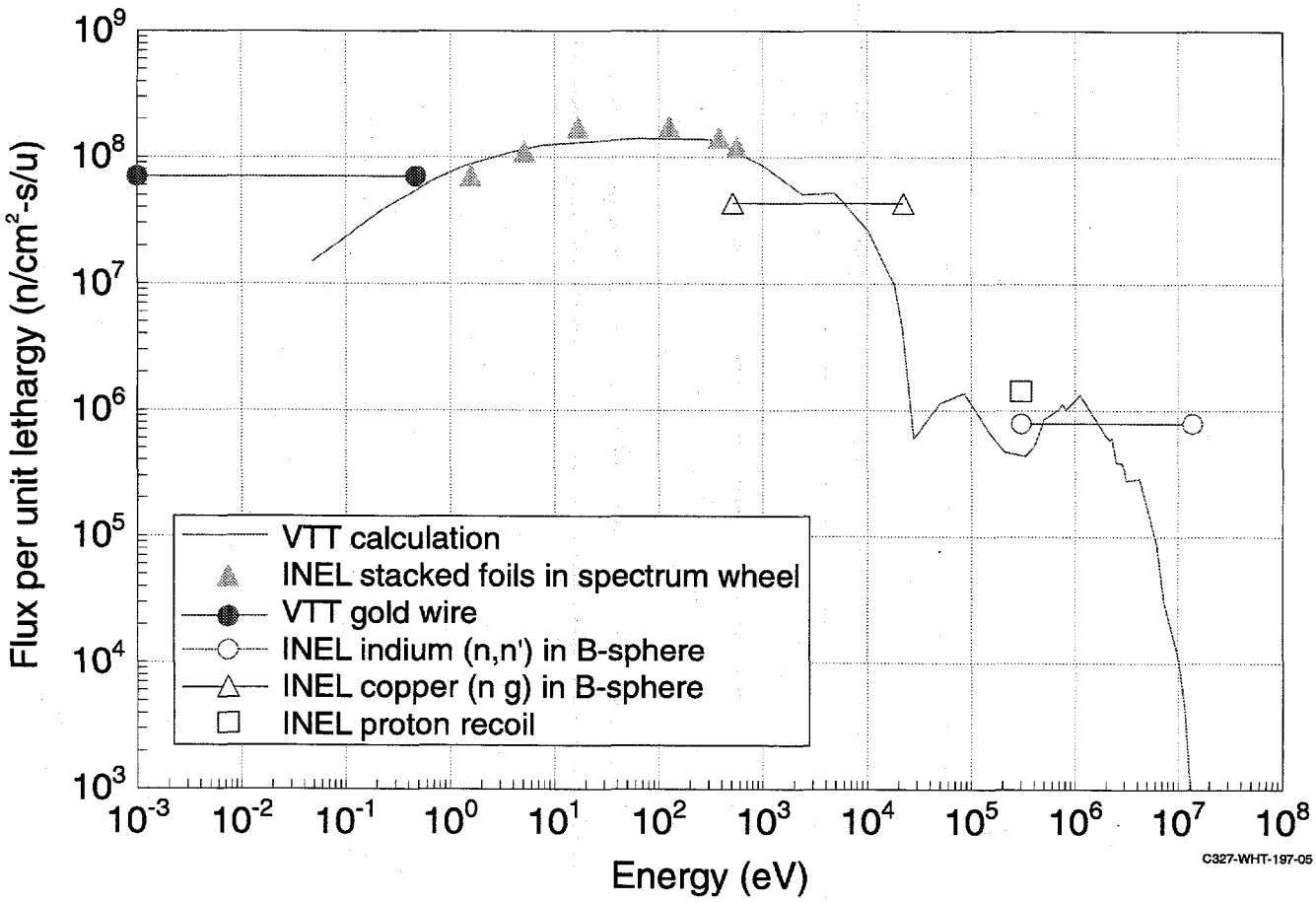


**Figure 13.** FiR1 free-beam spectrum, bismuth face, 250 kW, computed spectral data. The measured spectral data are computed at individual points and within the indicated ranges using various measurement techniques as indicated.

# REALTIME PATIENT MONITORING SYSTEM DEVELOPMENT

**Y. D. Harker, J. K. Hartwell, J. R. Venhuizen (INEEL)**

**W. Wanitsuksombut (Office of Atomic Energy for Peace, Bangkok, Thailand)[a]**

The objective of this work is to develop a small dosimetry system that can be read remotely in real time, so that medical personnel can monitor BNCT patient doses during a therapeutic irradiation. Presently available neutron dosimeters either are so bulky that their presence would perturb the therapeutic beam, or they cannot be read in real time.

The fiber-optic neutron dosimetry system being developed by PNNL scientists was tested again this year. INEEL and PNNL researchers, and the visiting scientist from Thailand conducted additional tests on the fiber-optic real time dosimetry system in the WSU research reactor. The results of these measurements were reported at the Zurich Conference in September 1996.[1]

### Scintillating Fiber Optic System

The technique developed by researchers at PNNL uses a small neutron sensitive fiber optic scintillation detector that has been used successfully in other applications.[2,3] In this device, a short (1 to 3 cm) length of neutron-sensitive fiber with a diameter of a few hundred micrometers is coupled to a fiber optic transmission line. Neutron (and gamma-ray) interactions in the scintillating fiber create light pulses that are transmitted to a set of detection electronics that scale the pulses and determine their rate. The detection rate is proportional to the neutron (and gamma-ray) dose rate.

[a] Visiting Scientist, Sponsored by the National Research Council, International Atomic Energy Agency

## MEASUREMENTS

INEEL, PNNL scientists, and the visiting scientist from Thailand participated in a measurement trip to the WSU TRIGA reactor facility to acquire test data on this dosimetry system under realistic neutron and gamma-ray dose conditions. The WSU reactor is configured with a number of beam ports to accommodate a variety of experiments; a description of the reactor was given in last year's report[4].

The neutron flux measurements were performed again using thin gold foils, bare and cadmium covered, to confirm the thermal and epithermal neutron fluxes within the experiment tube at 0.1 MW. The results of those measurements are given in Table 4. Five positions are identified; i.e., the 0, 6, 12, 18, and 24 inch positions. The position number indicates the approximate distance in inches from core centerline to the foil position in the beam port. The gamma ray intensities at the irradiation positions in the T3 beam port were determined by inserting a RadCal™ ion chamber probe. Measurements were conducted at the same reactor power and with the probe at the same positions as the gold foils. These results are also displayed in Table 4.

To separate the response of the candidate fiber optic dosimeters to neutrons and gamma-rays, a gamma-ray response curve was developed for the PNNL fibers. These calibrations were performed in the WSU $^{60}$Co gamma irradiation facility. This facility includes a strong $^{60}$Co gamma-ray source that can be remotely removed from a shielding cask. (The entire assembly is at the bottom of the reactor pool, thus the pool water provides an excellent personnel shield.)

Previously (1995), fiber-optic TLD probes, developed by International Sensors Technology (IST) Corporation had been tested at the same test facility.[4] The IST probe consists of a small TLD phosphor at the end of a fiber optic cable.

**Table 4.** Measured (8/96) neutron flux and gamma levels in the WSU reactor T3 beam port.

| Reactor power at 0.1 MW | | | |
|---|---|---|---|
| Position (inches) | Thermal flux[(a)] ($n/s/cm^2$) | RadCal™ Reading (rad/min.) | Gamma Dose to Neutron Fluence ($rad/n/cm^2$) |
| 0 | 1.10E+9 | 1144 | 1.73E-8 |
| 6 | 4.73E+8 | 1045 | 3.68E-8 |
| 12 | 1.72E+8 | 728 | 7.05E-8 |
| 18 | 6.51E+7 | 440 | 1.13E-7 |
| 24 | 4.35E+7 | 286 | 1.10E-7 |

(a) Thermal neutron fluxes determined using the 2200m/s cross section for $^{197}Au$ (98.7b) from the 1989 Chart of the Nuclides.

The fiber-optic cable serves as a link between the TLD phosphor and the laser light heat source, and the link between the phosphor and the luminescence light detector (photomultiplier tube). The laser heat source and the light detector assembly are contained in a small instrument case. The control of the laser heat, the acquisition glow curve response and the analysis of the data are performed by a laptop computer. The TLD phosphor used in these tests was magnesium borate. Two probes were used: one enriched in $^{10}B$ (a high neutron absorber) and one depleted of $^{10}B$. The $^{10}B$ probe is highly neutron sensitive and the other probe is predominately gamma sensitive. The results of 1995 test have been included in this report to make a comparison between the PNNL and IST methods.

Two PNNL fiber optic scintillator probes packages (labeled 807-1 and 813-a), differing in their active fiber length and the method of attachment to the transmission fiber, were irradiated in the characterized environment of the T-3 beam port. The probes were characterized by determining their neutron detection efficiency and their relative neutron to gamma ray sensitivities at varying photomultiplier threshold settings ranging at 30, 60 and 80 mV.

The PNNL fiber responses versus irradiation position and dectector threshold setting are given in Table 5. The IST TLD responses versus irradiation position are given in Table 6. Using the data from Tables 4, 5 and 6, neutron and gamma sensitivity coefficients were derived for the two PNNL fibers and the two IST TLD phosphors. These data are given in Table 7.

Varying the threshold setting on the PNNL fiber signal output is a viable way to vary the neutron to gamma response. From these results it appears that there is no benefit in using threshold settings greater than 60 mV. For the test environment where the gamma dose to neutron fluence ratio is $\sim 10^{-7}$ rads per $n/cm^2$, the neutron and gamma responses were very comparable. In this environment, a two threshold measurement approach is able separate the neutron and gamma components with reasonable accuracy. For the BNCT environment the gamma dose to neutron fluence ratio is in the $10^{-11}$ to $10^{-10}$ range. Based on the sensitivity coefficients in Table 7, the neutron to gamma response would be between 200 and 2000. Therefore, for the BNCT environment the PNNL fibers would function as neutron detectors with very little gamma interference.

**Table 5.** Measured PNNL fiber response versus. position and threshold setting[b].

| Fiber ID | Threshold Setting | Irradiation Position (inches) 0 | 6 | 12 | 18 | 24 |
|---|---|---|---|---|---|---|
| 807-1 | 30 mV | 2.76E+5 | 2.13E+5 | 1.39E+5 | 8.40E+5 | 4.96E+4 |
| | 60 mV | 8.81E+3 | 6.13E+3 | 3.20E+3 | 1.50E+3 | 7.25E+2 |
| | 80 mV | 1.12E+3 | 7.95E+2 | 3.98E+2 | 1.59E+2 | 6.61E+1 |
| 813-a | 30 mV | 5.83E+4 | 4.52E+4 | 2.97E+4 | 1.95E+4 | 1.21E+4 |
| | 60 mV | 6.18E+2 | 4.00E+2 | 2.28E+2 | 1.23E+2 | 7.22E+1 |
| | 80 mV | 6.29E+1 | 4.47E+1 | 2.71E+1 | 1.51E+1 | 9.04E+0 |

(b) All response values are in units of counts per second.

**Table 6.** Measured IST TLD response versus irradiation position[c].

| TLD | Irradiation Position (inches) 0 | 6 | 12 | 18 | 24 |
|---|---|---|---|---|---|
| Boron-10 | 1.40E+6 | 1.03E+6 | 6.13E+5 | 2.62E+5 | 1.18E+5 |
| Boron-11 | 5.11E+5 | 3.95E+5 | 2.76E+5 | 1.59E+5 | 1.02E+5 |

(c) All TLD responses are in units of charge.

**Table 7.** Neutron and gamma sensitivity coefficients for PNNL fibers and IST TLDs.

| Probe | Threshold Setting | neutron sensititity coefficient [c/(n/cm$^2$)] | gamma sensitivity coefficient [c/rad] | neutron to gamma sensitivity ratio [rad/(n/cm$^2$)] |
|---|---|---|---|---|
| 807-1 | 30 mV | 7.01E-5 | 1.04E+4 | 6.74E-9 |
| | 60 mV | 4.64E-6 | 2.02E+2 | 2.30E-8 |
| | 80 mV | 6.25E-7 | 2.42E+1 | 2.58E-8 |
| 813-a | 30 mV | 1.27E-5 | 2.30E+3 | 5.52E-9 |
| | 60 mV | 3.18E-7 | 1.42E+1 | 2.24E-8 |
| | 80 mV | 2.5-E-8 | 1.86E+0 | 1.34E-8 |
| IST B-10 | ---- | 6.07E-4 | 3.96E+4 | 1.51E-8 |
| IST B-11 | ---- | 1.07E-4 | 2.05E+4 | 5.24E-9 |

In the IST TLD case, the method used to separate neutron and gamma response is to utilize two probes with different neutron to gamma responses. For these tests one probe had a phosphor enriched in $^{10}B$ and the other had a phosphor enriched in $^{11}B$. Once again this concept did work very well for the test environment. For the BNCT environment the neutron to gamma response would large for both phosphors (e.g., ~100), which means that the response of both probes would be dominated by the neutron response. Using a two probe arrangement where one probe contains no boron (nor any other high neutron activation cross section material) and one that does contain boron appears to be an arrangement that is worth investigating.

## CONCLUSIONS

The results of these tests and those performed in 1995[4] have shown that the PNNL fiber-optic neutron detectors would be useful as neutron monitors for the real-time monitoring system. At their present stage of development, the PNNL detectors would not be able to do both neutron and gamma monitoring using just one probe per measurement location. (Using just one probe would be very desirable because it would reduce the volume needed to accommodate the probe(s).) At the current stage of the technology, a two probe approach appears to be the only viable alternative. The two probe concept could consist of a neutron sensitive PNNL detector and a gamma sensitive IST TLD or it could consist of two IST TLDs (one neutron sensitive and the other gamma sensitive).

## REFERENCES


1. M. Bliss, P. Reeder, and R.A. Craig, Y.D. Harker, J.K. Hartwell, and J.R. Venhuizen, *Progress Towards Development of Real-time Dosimetry for BNCT,* Proceeding of the 7$^{h}$ International Symposium for Neutron Capture Therapy, Zurich, Switzerland, Sept. 7-9, 1996.

2. "Glass-fiber-based neutron detectors for high- and low-flux environments", Mary Bliss, et.al., in *Photoelectric Detectors, Cameras, and Systems,* C. Bruce Johnson, Ervin J. Fenyves, Editors, Proceedings SPIE Vol. 2551, pp. 108-117 (1995).

3. "A Variety of Neutron Sensors Based On Scintillating Glass Waveguides", M. Bliss and R. A. Craig, in *Pacific Northwest Fiber Optic Sensor Workshop,* Eric Udd, Editor, Proceedings SPIE Vol. 2574, pp. 152-158, (1995).

4. INEL BNCT Research Program Annual Report 1995, pp. 70-73, J.R. Venhuizen, Editor, INEL-96/0139 (April 1996).

# MEASUREMENT DOSIMETRY SUPPORT

**O. R. Perry (INEEL)**

Significant progress was made in automation the gamma dosimety processing system supporting the INEEL BNCT program. The opportunity to automate the current system was available with the purchase of the Harshaw 6600E reader and TLD-REMS software to support other dosimetry programs on site. The new system provides for automated record keeping from preparation to final glow curve capture. The new system also provides the very significant advantage of capturing and providing BNCT dosimeter sensitivities that have been normalized to each other. With pre-established sensitivities, the normal preparation time for each BNCT event will be reduced by an estimated 80 person-hours. To support this new processing system, the BNCT program purchased 200 CaF: Mn dosimeters commonly called "chipstrates" and a pair of ND1.8 and ND2.1 filters (ND- neutral density) to protect the Photomultiplier Tubes (PMTs) from "shock" resulting from high dose irradiations. Advantages of the new BNCT gamma monitoring program include:

- Total electronic records capture
- Uniquely identifiable TLDs
- Pre-established phosphor sensitivities
- Reduced preparation time
- Reduced processing time and faster results reporting
- Moving the program from a 30 year old manually-based process system to a state-of-the-art TLD processor.

Phosphor sensitivity correction factors creation is expected to complete in early January 1997.

A BNCT irradiation conducted by ISU using Harshaw TLD-700 phosphors and Teledyne convex $CaF_2$:Mn disks were processed and reported to ISU. The convex calcium fluoride disks presented a special difficulty in processing and interpreting. Any additional irradiation experiments are expected to use the new phosphors listed above.

# 'TIDBIT' UPDATE

**C. A. Mancuso (Mancuso Consulting), J. R. Venhuizen (INEEL)**

The INEEL Database of BNCT Information and Treatment (TIDBIT) as been under development for several years. During 1994, TIDBIT got its name, underwent a complete change of appearance, had a major overhaul to the data structures that support the application, and system documentation was begun. A prototype of the system was demonstrated in September 1994. Additional enhancements have been made to the system as new releases of the interface software became available, and user input was used to make improvements. Since September 1996, a beta version has been in use to enter various patient data. The physical database still resides on a computer system located at WSU, and is assessable via the Internet.

## THE USER INTERFACE

The initial implementation of the database was started using tools that were character-based and function key intensive. Technology has advanced to the point where these types of user interfaces are no longer acceptable to the user community, and TIDBIT has been upgraded accordingly. The graphical user interface currently in use for TIDBIT is intuitive and does not require extensive training for proficient use.

In order to support research efforts that are being conducted across the country, the system has been designed to operate over the Internet. Users anywhere in the world can connect to the system using the desk-top platform of their choice (Windows 3.1 Macintosh, Motif, or character terminals). The thread that runs through the entire operation of the system is "point and click". From the main screen, the user selects the Patient Info module by pointing at the button with that label and clicking the mouse. The system then brings up the Patient Info screen. From there, there are other options that are "button" activated. The menu at the top of each form provides functions such as "Retrieve" and "Store." The user doesn't have to memorize anything.

The goal of TIDBIT is to collect planned and actual data in such a manner that the related parts are easily accessible. The following sub-systems provide the methods to store and retrieve related components.

### Names and Places

This module is used to specify the names and addresses of all project participants including researchers, veterinarians, physicians, patients, and research facilities. It also provides a method for relating these named entities.

### Patient Info

This module is used for keeping track of data related to a patient. It includes forms for planned procedures, actual results, admitting data, and clinical records. The system handles plans/results for drug administration, on-line MRI, PET, etc., image storage and retrieval, and neutron capture therapy doses and parameters. A cross-referenced search mechanism has been added that allows researchers to find information with some other identifying number, e.g., WSU clinic number.

### Analytical Chemistry

This module is used for correlating the tissue sample analysis with the irradiation data. In addition, this subsystem provides for the collection of detailed solution composition information.

### Reports

Presently this module has a few test reports. It can be expanded to generate reports of any of the stored date in any form desired. This module is expected to grow as researchers identify questions that require a different view for aggregation of the data.

### Sys Admin

This module is used by system administrators to maintain the reference table data. A primary objective in the data model was to provide validity checking on as many data fields as was practical. This option is used to keep the "valid choices" up todate and to grant permission to users.

## THE DATA STRUCTURES

As the user interface has evolved, so have their underlying structures- the tables and columns that comprise the database.

Originally, irradiations were planned to be a single fraction (one irradiation). A result of dog studies, treatment protocols were designed as multiple fractions- several irradiations separated by rest periods. Consequently the database had to be changed. The current structures can handle single infusion with multiple irradiations and multiple infusions with multiple irradiations. The tables also have space for the planned, working, and final irradiation data. These can be manual entries, or a worksheet can be used to calculate the working values.

The drug model assumes a solution has components which can be made up of quantities from different containers. These containers are then associated with a drug lot that identifies the manufacture and the name of the drug. Thus the researcher can identify, down to the specific container, each component of a solution that was given to a subject.

Analytic chemistry data is loaded directly from the spreadsheets that the chemists produce as a result of their analysis. Loading the data currently requires operator intervention, but methods for automating that process have been examined and may be implemented later.

## THE FUTURE

The database is available for field testing. Some of the historical animal data has been loaded into the database, and is available for report generation. The database can be cloned for special uses, e.g., human databases, etc., and password protection is available. User requirements and access information are available from the INEEL BNCT Program Office.